T Ü R K İ Y E
FIRAT UNIVERSITY
GRADUATE SCHOOL OF NATURAL AND APPLIED SCIENCES

THE EFFECT OF HIGH MELTING POINT ADDITIVE ELEMENTS ON CHARACTERISTIC TRANSFORMATION TEMPERATURES AND STRUCTURE OF CU-BASED SHAPE MEMORY ALLOYS

Hiwa Mustafa AHMED

Master's Thesis

DEPARTMENT OF PHYSICS
Division of General Physics

AUGUST 2020

T Ü R K İ Y E
FIRAT UNIVERSITY
GRADUATE SCHOOL OF NATURAL AND APPLIED SCIENCES

Department of Physics

Master's Thesis

THE EFFECT OF HIGH MELTING POINT ADDITIVE ELEMENTS ON CHARACTERISTIC TRANSFORMATION TEMPERATURES AND STRUCTURE OF CU-BASED SHAPE MEMORY ALLOYS

Author
Hiwa Mustafa AHMED

Supervisor
Assoc. Prof. Dr. Canan AKSU CANBAY

AUGUST 2020
ELAZIG

T Ü R K İ Y E
FIRAT UNIVERSITY
GRADUATE SCHOOL OF NATURAL AND APPLIED SCIENCES

Department of Physics

Master's Thesis

Title:	The Effect Of High Melting Point Additive Elements On Characteristic Transformation Temperatures And Structure Of Cu-Based Shape Memory Alloys
Author:	Hiwa Mustafa AHMED
Submission Date:	13 July 2020
Defense Date:	13 August 2020

THESIS APPROVAL

This thesis, which was prepared according to the thesis writing rules of the Graduate School of Natural and Applied Sciences, Fırat University, was evaluated by the committee members who have signed the following signatures and was unanimously approved after the defense exam made open to the academic audience.

Signature

Supervisor:	Assoc. Prof. Dr. Canan AKSU CANBAY Firat University, Faculty of Science	Approved
Chair:	Assoc. Prof. Dr. Canan AKSU CANBAY Firat University, Faculty of Science	Approved
Member:	Prof. Dr. Fahrettin YAKUPHANOĞLU Firat University, Faculty of Science	Approved
Member:	Prof. Dr. M. Enver AYDIN Dicle University, Faculty of Science	Approved

This thesis was approved by the Administrative Board of the Graduate School on

..... / ..... / 20 .....

Signature

Prof. Dr. Soner ÖZGEN
Director of the Graduate School

DECLARATION

I hereby declare that I wrote this Master's Thesis titled " The Effect Of High Melting Point Additive Elements On Characteristic Transformation Temperatures And Structure Of Cu-Based Shape Memory Alloys" in consistent with the thesis writing guide of the Graduate School of Natural and Applied Sciences, Firat University. I also declare that all information in it is correct, that I acted according to scientific ethics in producing and presenting the findings, cited all the references I used, express all institutions or organizations or persons who supported the thesis financially. I have never used the data and information I provide here in order to get a degree in any way.

13 August 2020

Hiwa Mustafa AHMED

PREFACE

I feel very honored to complete this thesis work by which, I believe, new scientific knowledges are revealed about the nature of shape memory alloys, which alloys are very important and beneficial smart materials employed vastly in today's advanced technological and industrial applications due to exceptional features and functionalities of these alloys. The operational working temperatures of shape memory alloys are demanded to be enhanced up in various practical applications. The addition of some dopant elements to shape memory alloys is one of the ways to solve this problem. In this work, the operational working temperatures of Cu-based shape memory alloys are presented to be escalated by minor additions of extra alloying metal elements. Obtained results can be useful in high-temperature shape memory applications.

During all of my mastering process;

Firstly, I'm grateful to God for good health to complete this thesis, I especially thank my supervisor Assoc. Prof. Dr. Canan AKSU CANBAY for her huge supports and enlightening advice she gave me during every stage of this thesis work. I would like to thank my family members, my wife Renaz Qadir she was supported me. All the friends who supported me and helped me, very especially Mr. Oktay Karaduman.

Thanks, everyone.

This work was supported by the Management Unit of the Scientific Research Projects of Firat University (FUBAP), **Project Numbers: FF.19.12**.

Hiwa Mustafa AHMED
ELAZIG, 2020

TABLE OF CONTENTS

Page

ABSTRACT

The Effect Of High Melting Point Additive Elements On Characteristic Transformation Temperatures And Structure Of Cu-Based Shape Memory Alloys

Hiwa Mustafa AHMED

Master's Thesis

FIRAT UNIVERSITY
Graduate School of Natural and Applied Sciences

Department of Physics

August 2020, Page: xii + 48

In this thesis work, four types -one ternary and three quaternary- of Cu-based shape memory alloys (SMAs) with new different compositions of Cu-17.33Al-4.74Fe-2.08Mn (at.%), Cu-20.82Al-3.53Fe (at.%), Cu–18.73Al–21.06Be–0.13Mn (at. %) and Cu–12.9Al–22.73Be-0.37Mn (at.%) were produced by arc melting method. At first, the high purity (99.99 %) copper, aluminum, iron, beryllium, and manganese elements in powder forms were mixed and then formed into pellets by applying pressure and these pellets were melted in an arc melter to get as-cast ingots. The alloy samples obtained by cutting these ingots were heat-treated at 900 °C for 1h and right after quenched in traditional iced-brine water to form of β1' martensite phase in the alloy samples. In this way, the alloys were acquired shape memory effect property. Then the thermodynamic parameters and characteristic martensitic transformation temperatures of the alloys were detected by differential thermal analysis (DTA) measurements and differential scanning calorimetry (DSC) taken at different heating/cooling rates. The DSC results showed that the characteristic martensitic transformation temperatures of the alloy samples all became in the range of 100–400 °C by the effect of additive elements, so this means that each one of these alloys is to be defined as a high temperature shape memory alloy (HTSMA). The DTA results showed that the thermal behaviors of these alloys in high-temperature region became in accord with those of other Cu-based SMAs. Also, the other kinetic parameters related to the martensitic transformations of the alloy samples such as entropy, equilibrium temperature, enthalpy and activation energy were determined. As to structural measurements taken at room temperature, the formation of the martensite phases was detected in all of the alloy samples by XRD results and by optical micrographs.

Keywords: Cu-based shape memory alloys, High-temperature shape memory alloys, Shape memory effect, Martensitic transformations, Activation energy, Differential calorimetry

ÖZET

Yüksek Erime Sıcaklıklarına Sahip Katkı Elementlerinin Cu-bazlı Şekil Hafıza Alaşımlarının Yapı ve Karakteristik Dönüşüm Sıcaklıklarına Etkileri

Hiwa Mustafa AHMED

Yüksek Lisans Tezi

FIRAT ÜNİVERSİTESİ
Fen Bilimleri Enstitüsü

Fizik Anabilim Dalı

Ağustos 2020, Sayfa: xii + 48

Bu tez çalışmasında, sırasıyla Cu-20.82Al-3.53Fe Cu-17.33Al-4.74Fe-2.08Mn (at.%), (at.%), Cu–18.73Al–21.06Be–0.13Mn (at.%) ve Cu–12.9Al–22.73Be-0.37Mn (at.%) kompozisyonlarına sahip biri üçlü ve üçü de dörtlü olmak üzere toplam dört farklı tip Cu-bazlı şekil hafızalı alaşım (ŞHA) ark eritme metoduyla üretilmiştir. İlk etapta, toz halindeki yüksek saflığa (99.99 %) sahip bakır, alüminyum, demir, berilyum ve manganez elementleri karıştırılıp basınçla peletler halinde elde edildi ve sonra bu peletler bir ark eriticisinde eritilerek külçe halinde dökümleri yapıldı. Bu külçelerin kesilmesiyle elde edilen alaşım numuneleri 900 °C'de 1 saat ısıl işleme tabi tutulduktan hemen sonra geleneksel tuzlu buzlu suya daldırılarak bu alaşımlarda β1' martensit fazının oluşması sağlandı. Bu sayede alaşım numunelerine şekil hafıza özelliği kazandırıldı. Sonra bu alaşımların termodinamik parametreleri ve karakteristik martensitik dönüşüm sıcaklıklarının belirleyebilmek için farklı ısıtma/soğutma hızlarında alınan diferansiyel taramalı kalorimetri (DSC) ve diferansiyel termal analiz (DTA) ölçümleri yapıldı. DSC sonuçları alaşım numunelerinin karakteristik martensitik dönüşüm sıcaklıklarının katkı elementlerinin etkisi ile 100-400 °C aralığına yükseldiğini gösterdi ki bu da bu alaşımların her birinin birer yüksek sıcaklık şekil hafızalı alaşım (YSŞHA) olarak tanımlanması gerektiği anlamına gelmektedir. DTA sonuçları, bu alaşımların yüksek sıcaklık bölgesindeki termal davranışlarının diğer Cu-bazlı ŞHA'larınkiyle uyum içinde olduğunu gösterdi. Ek olarak entalpi, entropi, denge sıcaklığı ve aktivasyon enerjisi gibi alaşım numunelerinin martensitik dönüşümleri ile ilgili diğer kinetik parametreler de belirlendi. Oda sıcaklığında alınan yapısal ölçümlere gelince, XRD sonuçları ve optik mikrograflar ile tüm alaşım numunelerinde martensit fazlarının oluştuğu tespit edildi.

Anahtar Kelimeler: Cu-bazlı şekil hafızalı alaşımlar, Yüksek sıcaklık şekil hafızalı alaşımları, Şekil hafıza etkisi, Martensitik dönüşümler, Aktivasyon enerjisi, Diferansiyel kalorimetri

LIST OF FIGURES

Page

LIST OF TABLES

Page

SYMBOLS AND ABBREVIATIONS

Symbols

A_s	Austenite start temperature
M_s	Martensite start temperature
A_f	Austenite finish temperature
M_f	Martensite finish temperature
E_a	Activation energy of martensitic transformation
e/a	Average valence electron concentration per atom
D	Crystallite size
T_o	Equilibrium temperature
$A \leftrightarrow M$	Austenite ↔ Martensite
V	Volume
P	Pressure
E	Total energy
H	Enthalpy
S	Entropy
T	Temperature
G	Gibbs free energy
β	Beta phase
α	Alpha phase
γ	Gamma phase

Abbreviations

SMA(s)	Shape Memory Alloy(s)
SME	Shape Memory Effect
SE	Superelasticity
EDX	Energy Dispersive X-ray spectroscopy
SEM	Scanning Electron Microscope
DTA	Differential Thermal Analysis
TGA	Thermogravimetric analysis
FWHM	Full Width Half Maximum
OWSMA	One Way Shape Memory Alloy
TWSMA	Two Way Shape Memory Alloy
HTP	High-Temperature Phase
LTP	Low-Temperature Phase
MT	Martensitic Transformation
RT	Reverse Transformation
XRD	X-Ray Diffraction
TMT	Thermoelastic Martensitic Transformation
EDX	Energy Dispersive X-Ray
LIS	Lattice Invariant Shear

1. INTRODUCTION

Nowadays smart materials are increasingly used in numerous advanced technological applications. Shape memory alloys (SMAs) are a unique kind of smart materials that can keep in mind their original shape after deformed plastically by thermo-mechanical loads. By heating, these alloys in deformed shapes experience a kind of solid to solid phase transformation which leads them to revert their original shape without applying any load. Such direct and reverse phase transformations are known as martensitic transformations which occur between two solid phases called martensite and austenite phase. The martensitic transformation that occurs as austenite ↔ martensite (A↔M) inter-transition is the underlying mechanism responsible for interesting properties of SMAs, for example, shape memory effect (SME) and pseudoelasticity (superelasticity) properties. Numerous alloys are owning a special characteristic to these transformations such as NiTi, Cu-based, and Fe-based shape memory alloys.

Background historical good for understanding in every science, shape memory was first described by the stages concerningthe find of the shape memory effect (SME) was taken within the 1930s, when Swedish physicist Arne Ölander found the pseudoelastic activities of the Cd-Au alloy in 1932 [1]. Moradian and Greninger [2] were identified the procedure and disappearing of a martensitic phase via increasing besidesdecreasing the heat of a Zn-Cu alloy. The fundamental phenomenon of the memory effect directed by the thermoelastic behavior of the martensitic phase was generally detailed a decade afterward by Khandros and Kurdjumov [3] additionally by Read and Chang [4]. Within the 1962s, Buehler and his co-workers at the U.S. Naval Ordnance Laboratory found the shape memory effect (SME) within the binary alloy of titanium in addition to nickel, which can be measuredan innovation within the arena of shape memory materials. This alloytile now has important properties was known as Nitinol. The utilize of NiTi is interesting since of its uncommon useful behavior, which is totally modern compared with the other customary metal alloys [2].

Shape Memory Alloys (SMAs) owing to their unique and superior properties are one of the branches of the smart material family tree; they are also called as smart alloys, memory alloys, memory metals, muscle wires, and smart metals. A shape memory alloy is a microtome alloy therefore as to remember initial or real shape when heated or deformed from plastic deformation [3, 4] . Nowadays SMAs have a high place in the scientific field from both industrial and medical because it has unique properties high power to mass and stroke length to mass ratios, a combination of sensor and actuator elements in a single component, clean, debris-less, spark-free, silent operation and capability of operating in zero gravity, controlled accelerations [5]. SMAs have found wide usage in hydraulic, pneumatic and motor-baked systems, aerospace and

actuators. These alloys contain applications to robots and automobile, aerospace as well as biomedical applications.

Physical phenomena behind hand and their applications are also debated refer to a unique class of alloys that reminisce their original shape (or pre-deformation shape) when increasing heat from some relatively low temperature. By heating process, the results achieve in a reversible phase transformation from a weaker to a stronger phase, surveyed by an associated recovery of all the gathered strain [5]. The strain recovery can take place alongside of big forces where applied, such as use in their application as actuators. Indeed, in spite of the fact that numerous alloys are found to show the shape memory effect, as it were those alloys that came back a significant sum of strain are of prime significance. These include TiNi alloys and copper-based alloys such as Cu-Al-Ni- and Cu-Al -Zn [5]. Mostly SMAs exhibit martensitic transformation (operational temperatures of SMAs) at temperatures below 100 ºC. For example, cardiovascular NiTi stents work at around body temperature at where these SMA devices operate by their martensitic transformation resulting in shape change by strain recovery induced by blood heat. But SMAs with certain higher martensitic transformation temperatures are muchly demanded in some industrial applications, too. To modify or increase transformation temperatures researchers use some methods such as adding some extra elements in SMA systems or performing heat treatment on SMAs.

High-temperature shape memory materials (HTSMMs) classify to three groups of change temperature, to begin with a group within the variety of 100–400 ºC, second group within the range between of 400–700 °C; and final group over 700 ºC [6, 7].

In this thesis work, one ternary and three quaternary Cu-based shape memory alloys with different compositions of Cu–18.73Al–21.06Be–0.13Mn (at.%), Cu–12.9Al–22.73Be-0.37Mn (at.%), Cu-17.33Al-4.74Fe-2.08Mn (at.%) and Cu-20.82Al-3.53Fe (at.%) were produced by arc melting method. Then, in order to search out their SMA properties the alloys were characterized by structural XRD, EDX and optical microscopy measurements and differential calorimetry (DSC and DTA) tests.

2. SHAPE MEMORY EFFECT

Shape memory effect (SME) is a very important process in shape memory alloys (SMAs) and they have three crystal structures (detwinned martensite, twinned martensite, austenite, and martensite) as shown in Figure 2.1. Mutual inter-convertibility of martensite and austenite phases of SMAs depends on heat. The austenite phase has a higher symmetry with cubic structure while the martensite phase has lower symmetry and is relatively soft and easily deformed. In the SME, martensite phase crystal structural changes from twinned martensite to another structural called detwinned martensite by adding an external load, this transformation occurred due to crystal transformation and it is atomically diffusionless, only crystal structure changes without change in chemical composition. The previous is related with the recovery from loading-originated strains of up to 8% or 10% for NiTi [8] and 4-5% for iron-based and copper-based alloys [1] without significant leftover strains [8-11]. The impact is characterized by the capacity of recuperating leftover strains created after cyclic loading with a temperature variety. SMAs are characterized by four characteristic martensitic phase transformation temperatures as M_f, M_s, A_s and A_f ; M symbol for martensitic phase, s and f respectively for start and finish temperatures, also A symbol for austenite phase (high-temperature phase). Each of these counterpart M and A phases starts to form in its counterpart phase at start temperature and formation is fully completed isostatically as reaching at finish temperature. Every SMA has its specific martensitic transformation temperatures.

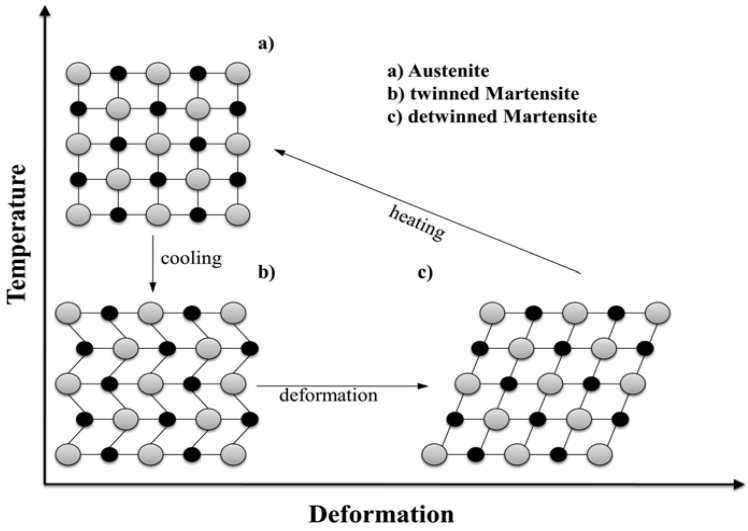

Figure 2.1. Schematic illustration of crystal structure in the martensite and austenite phase [12].

In Figure 2.1. we can see the structure of shape memory variation with the change in temperature. In the first case shown in this diagram modeled by the measuring variables of

temperature that goes on Y-axis and of deformation that goes on X-axis, at high temperature the crystal structure at austenite phase is high symmetry phase, by cooling this crystal structure changes to twinned martensite phase and then by mechanical load or pressure (by deformation) twinned martensite changes to detwinned martensite and lastly, this detwinned martensite can be converted back to austenite again by heating. Having looked at this cycle of phase transition steps seen in Figure 2.1 the cycle goes on when temperature or deformation changes the crystal structure without a change in chemical properties [4].

2.1. One – Way Shape Memory Effect

Within the one-way shape memory effect (OWSME) the material or alloy training to recover its original shape at high temperature (austenite phase) i.e. to reminisceits original shape by the formation of austenite phase (above A_s temperature), the ratio of recovery depending on temperature starts from A_s to A_f After the alloy in low-temperature martensite phase and with its original shape is deformed by the external mechanical load, it again earns its pre-deformation shape by the formation of austenite phase by increasing heat, as seen in Figure 2.2. This figure (a-d) illustrates OWSME mechanism in bar SMAs step by step respectively as; (a) this bar SMA at low-temperature martensite state has regular bar shape (original shape) before deformation or bending, (b) it is deformed and bent in martensite state at low temperature smaller than the A_s, (c) then the deformed shape is recovered to the original shape by applying heat (by increasing temperature) and (d) by cooling bar SMA the austenite phase completely changes to martensite phase at low temperature smaller than the M_f without a change in shape i.e. it does not change to the deformed shape again.

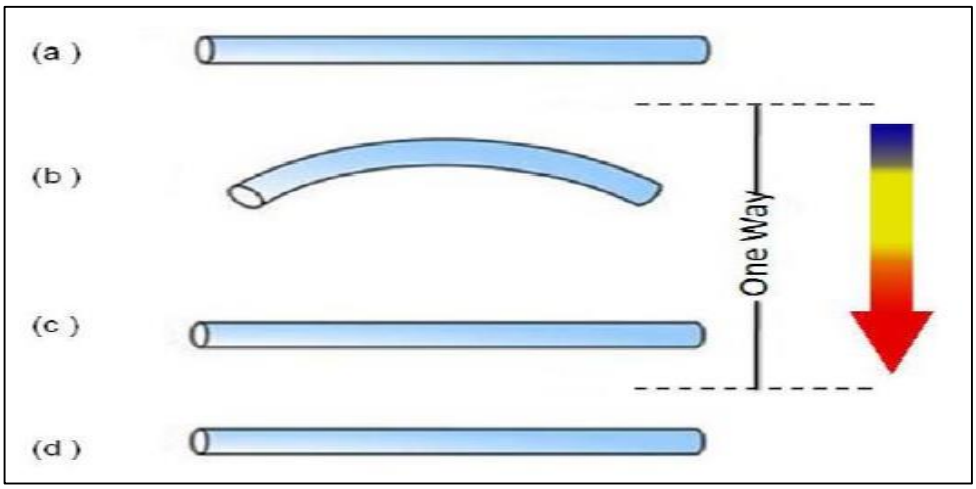

Figure 2.2. Macroscopical process of one-way shape memory effect (a) martensite, (b) loaded and deformed phase at M_f,≥T (c) as austenite T≥A_S, (d) cooling M_f ≥T [9].

2.2. Two – Way Shape Memory Effect

Most of the present applications of shape memory alloys are based upon OWSME memory that is the ability to remember the first original shape after deformation when reaching a high temperature. In many cases SMA can be appropriately trained to get two-way shape memory (TWSME), the material presently remembering pre deformation phase at both austenite and martensite phases. Within the two-way shape memory alloys (TWSMA), they appear reversible transformation behavior both during heating and cooling. This behavior is presented in the material by thermo-mechanical training. The impact stabilizes amid the fixing cycles within the chosen orientations of the martensite. These outcomes in remaining stress levels within the SMAs, which put on the least stress to reset the SMAs through itself. Amid the training prepare, the actual two-way SMA element is deformed to its yield strength in together the martensitic and the austenitic state [12]. Figure 2.3 shows the TWSMA macroscopically from (a-d) respectively, shape in (a) it is bars trained as shape memory alloy in cold stated martensite phase $T \leq M_f$, (b) that is the same material but was trained as a bent state at low temperature. Within the TWSMA, the material training to recovery to original shape after the deformation and can back to the original shape in two phases as shown in (c) and (d).

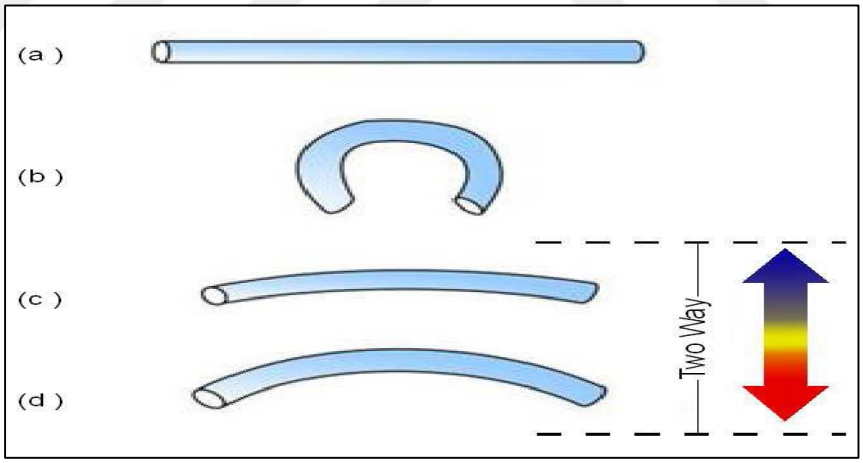

Figure 2.3. The macroscopically process of two-way shape memory effect (a) martensite state $T \leq M_S$, (b) loading and deformed at martensite, (c) as austenite state $T \geq A_S$, (d) cooling $T \leq M_S$ [9].

2.3. Pseudo-elasticity

Superelasticity or pseudo-elasticity is thermo-mechanic behaviors and another special property of assured shape memory alloys. Dissimilar to shape memory effect, pseudoelasticity occurs in a limited extent of temperatures above the A_f, when stress increased on shape memory alloys, the microstructures (crystal structure), and therefore macroscopic shape deform, after reducing the load both of them can recover to original shape [13]. Pseudoelasticity has two types

of crystal structure; unload state is austenite cubic crystal structure and load state is detwinned martensite structure. When loaded at a high temperature greater than the A_f, a macroscopic deformation occurs due to that crystal structure changes microscopically from cubic to detwinned martensite phase and after then by reducing load or stress the crystal structure changes to austenite phase again which leads macroscopic shape to recover back to the original shapes, as appeared in Figure 2.4 [5, 12, 14].

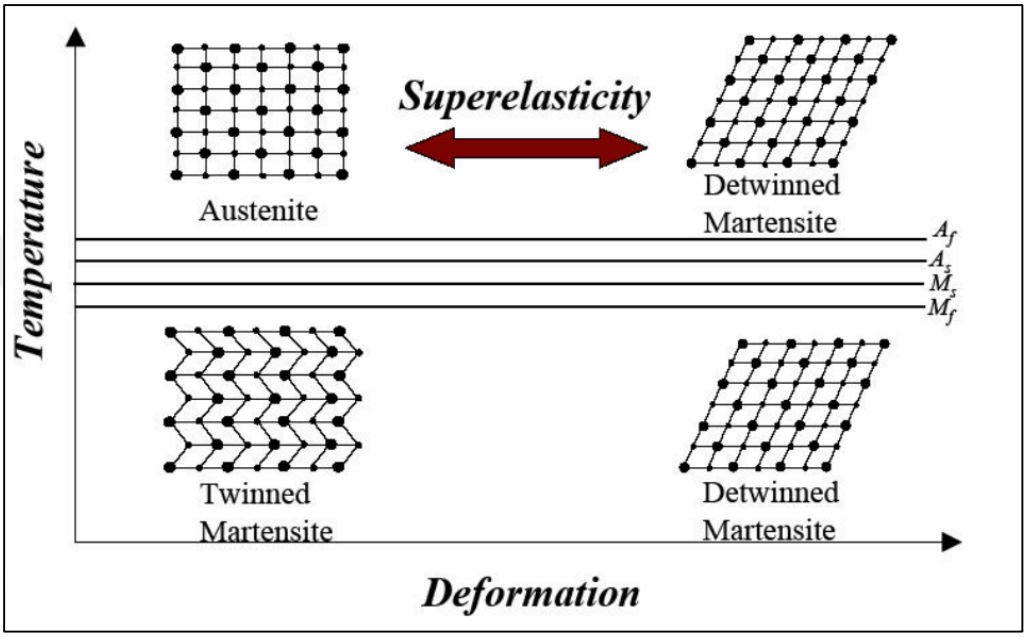

Figure 2.4. Pseudoelasticity behavior of shape memory alloys [14].

2.4. Stress-Strain Effect On SMAs

At low temperatures, SMAs are in martensite phase formed by martensite twins that observed in the crystal structure as shown with point-B seen in Figure 2.5. After increasing mechanical load or stress the SMAs deform by phase arrangement and change to detwinned martensite, with remaining the same strain on the shape, seen at point-C in Figure 2.5. The deformation before faulting at plastic deformation region is the main criterion for shape memory alloy behavior and at this region, any alloy cannot be recovered to original shape but when temperature increased in SMAs the plastically deformed shape macroscopically reverts to original pre-deformed shape by reason of microscopically phase change from detwinned martensite to high symmetry austenite phase as shown with point-A in Figure 2.5. The amount of recovery depends on the type of SMAs and quantity of temperature and this can be observed in the cycle of stress-strain-temperature appeared in Figure 2.5 [4].

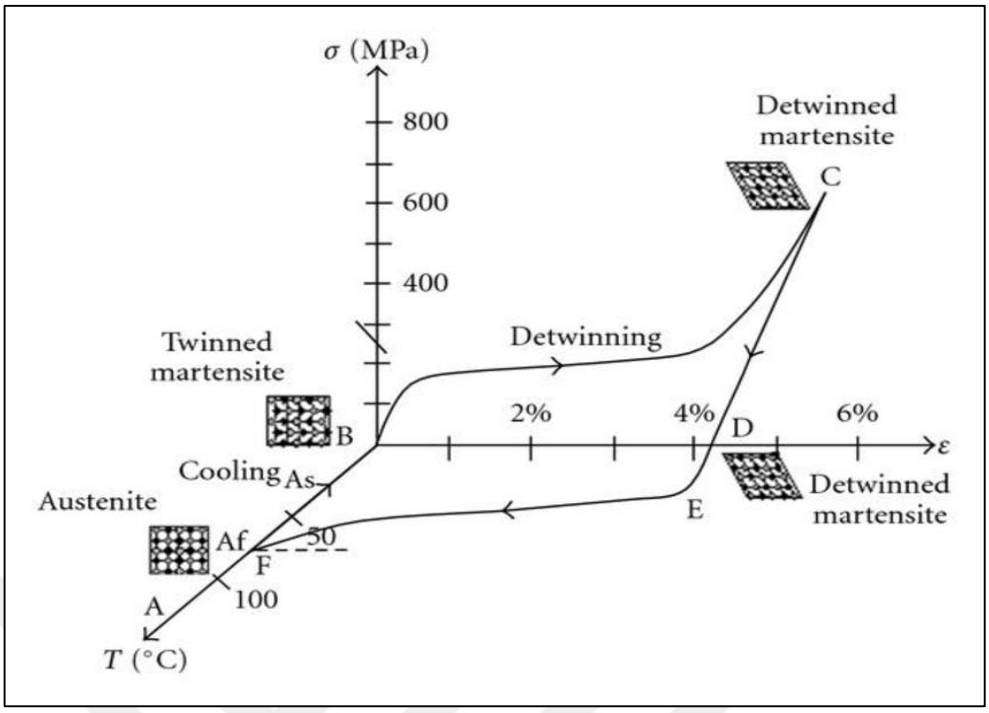

Figure 2.5. Stress-Strain-Temperature cycle in SMAs [15].

2.5. Martensitic Transformation

In some metallic systems, the alteration in crystal structure occurs by a homogeneous deformation of the parent phase, called martensitic transformations, which are diffusionless. Martensite phase transformation occurs in solid-state which involves variation in crystal structure but the chemical properties are stable [16]. So this phase change involves no longer diffusion and known as diffusionless transformation, the transformation from martensite to austenite or contrariwise is related to the absorption and release of latent heat [4]. This type of reaction includes a type known as the martensitic transformation. It was first discovered in steel by quenching austenite phase and the resultant phase was named in German scientist Adolf Martens. Martensite is a state of the material at a low temperature. The formation of martensite structure is spontaneous through a shearing movement of atoms when an alloy quenched exceptionally quickly through solid-solid phase change extend to a low temperature, it is frequently possible to completely smother the arrangement of the low-temperature adjust stage or the arrangement of any metastable low temperature. The martensite transformation in many alloys only naturally occurs with slow cooling rates without the need for rapid quench as in steel [4].

The martensitic transformation (MT) arise is a diffusionless transformation defined via a shear-like mechanism or change the arrangement of atoms in crystal structure. The parental (austenite) phase (high-temperature phase) is generally cubic [17]. From parent phase, the structure changes into the martensite phase (lower-temperature phase) by way of lower

symmetrically, as seen in Figure 2.6 (a and b). The martensite phase at low temperature has a different crystal structure, first before the deformation called the twinned martensite phase (Figure 2.6-b) and the second after deformation called detwinned martensite alteration (Figure 2.6-c) [12].

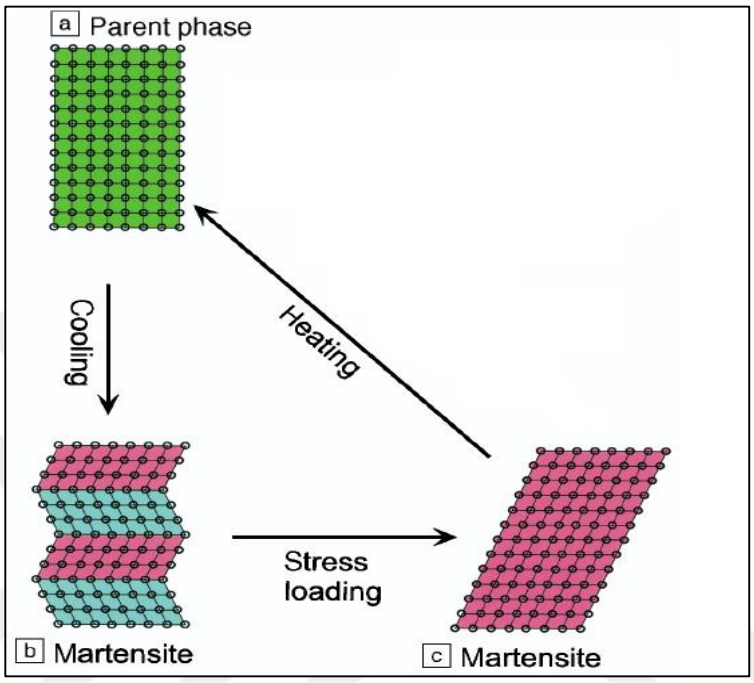

Figure 2.6. The chart representation of SME [12]. a) parent (austenite) phase, b) twinned structure of martensite phase and c) stress induced detwinned martensite.

The parent phase (cubic structure) has advanced symmetrically more than the martensitic phase, multiple formations of martensite have a similar structure in dissimilar orientations and it is possible in order to hold elastic strains about the martensites and this is called self-accommodation. The two neighbor variations are twin-correlated to each other and may possibly contribute to distortion if the interface is mobile under stress. The martensitic transformation is distributed into two types: thermoelastic and nonthermoelastic. The thermoelastic transformation is categorized by a small temperature hysteresis, a crystallographically reversible transformation and a movable twin interface [17].

2.6. The Characteristic of Martensitic Transformation

The characteristic of martensitic transformation can be affected and modified, leading to changes in alloy behavior, by many things such as the crystal structure of alloy composition and structure, effect off applied stress, orientation relation, reversibility of transformation and amount of transformation with time and dependence of temperature [4].

2.7. Thermoelastic Martensitic Transformations

The wonderful behavior of SME and superelasticity (SE) of shape memory alloys depending on the temperature reliant on austenite altering to the martensite phase occur in micro scales, which is commonly named thermoelastic martensitic transformation (TMT) by a shear-like component as seen in Figure 2.7. The different orientations in areas A and B as shown in Figure 2.7 are called as the correspondence variation of the martensite (lower symmetry), numerous variations can be formed from the same parent (austenite) phase. If the temperature is high and the martensite becomes unstable and in this case the lattice crystallography is reversible, therefore the reverse transformation (RT) happens i.e. the martensite returns to the parent phase within the pre-deformation orientation [18].

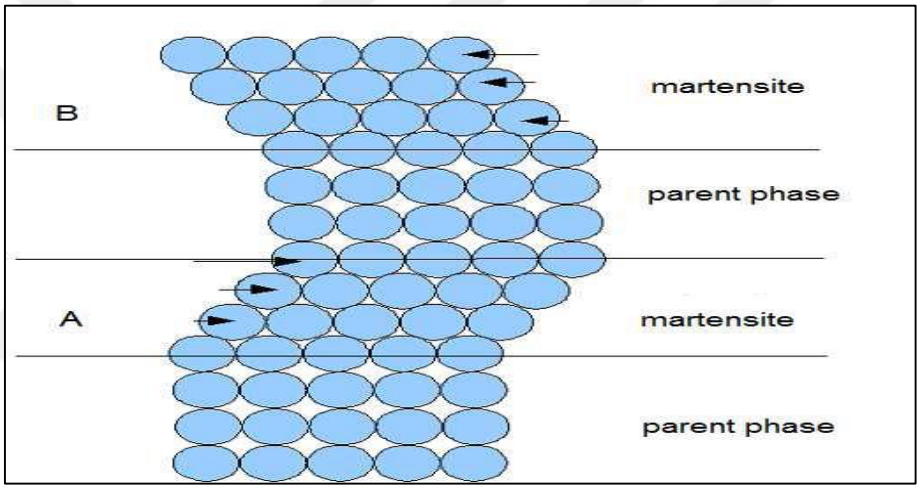

Figure 2.7. Martensitic Transformation in two dimensions [9].

In a crystallographic backdrop, the phase transformation since austenite to martensite is occurs of change in two components; the lattice invariant shear and the Bain strain. These mechanisms in crystallography are very multifaceted. Also, they are conceivable to clarify in a very basic way utilizing a two–dimensional axis. The Bain strain, to be specific for lattice deformation comprises an arrangement of atomic movements on a little staircase that it transports to the arrangement of a different phase. Hence, in spite of the fact that the bain strain is complex, the combined impact of the bain strain and lattice doesn't alter the shear and change over the macroscopic strain into a shear. In truly, martensite transformation is related to a shape alter combined with a large strain emerges all over within the martensite. When it is shaped in the austenite stage to diminish the strain is vital within the advanced forms of MT, the component to get is called lattice invariant shear (LIS). There are two conceivable LIS mechanisms twinning and slip as shown in Figure 2.7. Twinning or slip could be a required process in martensite

transformation, which be influenced by upon the kinds of alloys, but twinning is ordinarily presented as a LIS in SMA [9, 19].

Therefore, in twinning, created by appropriate shear, in specific, two twin crystals are correlatedvia a symmetry process with admiration to a reflecting plane, so-called twin boundary plain as shown in Figure 2.8. Crystal twinning happens aftertwo isolated crystals share a few of the similar crystal lattice focuses in a symmetrical way. The result is an associate development of two crystals in a variability of particular arrangements isolated via twin boundary surface [9].

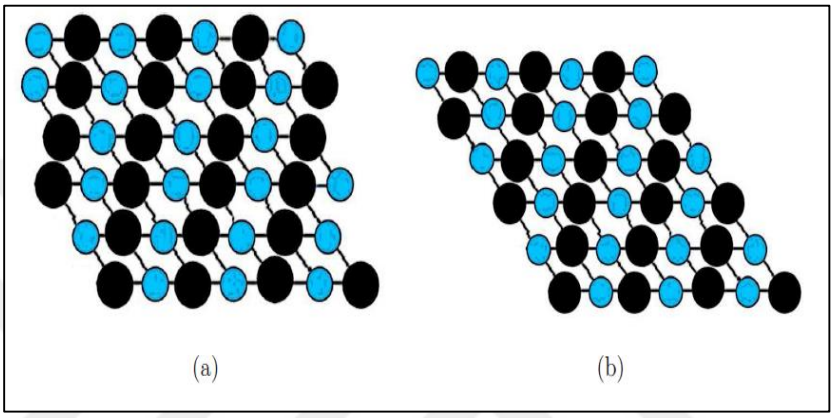

Figure 2.8. Twinning and slip mechanisms in martensite: (a) slip mechanism in martensite (b) twinning mechanism in martensite SMA [9].

Twin boundaries (Figure 2.9) happen while two crystals of the similar kind intergrowth consequently that as it was a small misorientation occurs amid them, the atoms arranged on that twin boundary get a similar amount besides kind of bonds in together directions [4, 9].

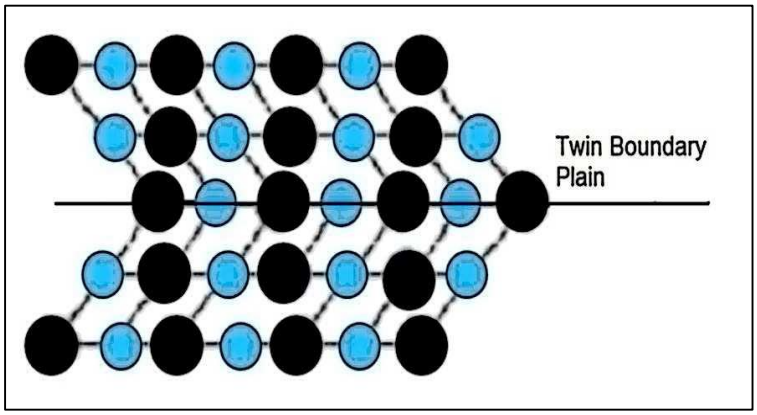

Figure 2.9. Plain of twin boundary martensite [9].

In fact, increasing stress to twinned structure boundaries will smooth move from many variants twinned to single variant detwinned with macroscopically deformation (Figure 2.10 (a-

c)). Using a two–dimensional system, Figure 2.10 clarifies to show microstructures, (a) austenite phase (b) twinned martensite phase many variants and (c) single variant detwinned crystal structure produced by applying stress [20]. The twinning and deepening processes are typically mechanisms utilized in SMA, these microscopical mechanisms are the basis for clarifying the plainly visible SMA properties [9].

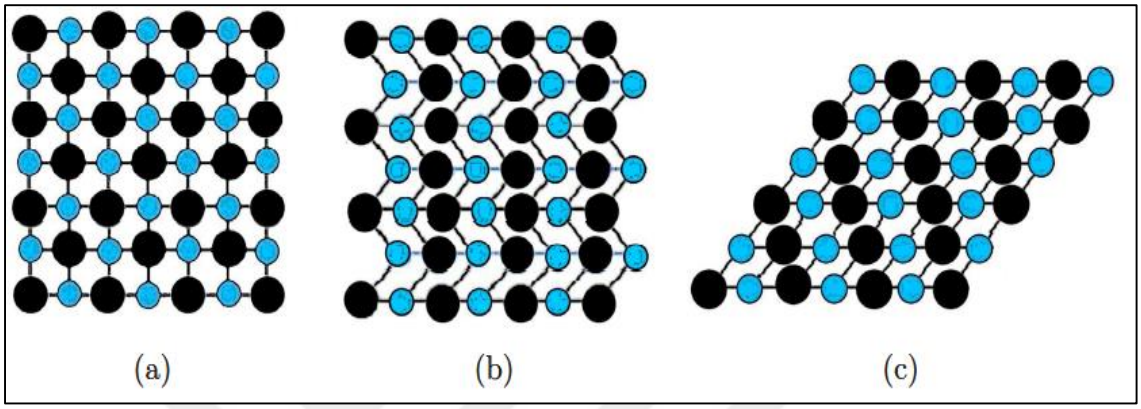

Figure 2.10. Technique: Austenite and martensite microstructure is shown in two–dimensions; (a) cubic structure of high-temperature austenite, (b) twinned lattice structure of low-temperature martensite, (c) detwinned martensite at low temperature [9].

2.8. Thermodynamics of Martensitic Transformation

The application of thermodynamics to clarify of the martensite transformation was made for the first time when it was observed in some iron alloys as the martensite to austenite transformation or contrariwise is dependent of latent heat absorption and release [21]. In fact, the variations in the structural morphology due to effective thermodynamic parameters, a number of particular characteristics of martensite transformation ought to be reflected in applying thermodynamics. Perhaps the greatest important point is that the stability participatory in this kind of phase transformation is a metastable one and by definition will certainly not be attainable for estimation of the accurate associated with thermodynamic quantities. Accordingly, a show need be created for each alloy framework of interest, certified within the regions for which test information exists and used to achieve the entire free energies of the individual phases as a work of temperature, composition, and pressure a second characteristic is that martensitic changes happen through any introductory isolate of combination components in the event that one but the bainitic transformations from the type. This conservation of consistent composition done the transformation simplicities the calculations by authorizing the utilize of the single component or pseudosingle component calculations to the transformation. Hence, once the temperature necessity of the Gibbs free energy of both the austenite and martensite phases is known at a settled composition [21].The chemical-free energy of the martensite phase to be less than the

chemical-free energy of the austenite phase causes austenite→martensite conversion. In order the external transformation in martensitic transformation, the energy must be free enough to do the conversion. The driving force of martensitic transformations is basically this free energy difference, this energy called Gibbs free energy.

The thermodynamic equilibrium temperature T_o is related to characteristic transformation temperatures and it is the temperature where free energies of two phases are equal. We can determine this parameter in two different formulas. The formula of T_o equilibrium temperature according to Salzbrenner and Cohen [22] is given as below;

$$T_o = 1/2(M_s + A_s) \tag{2.1}$$

and according to Tong and Wayman [22] it is formulated as;

$$T_o = 1/2(M_s + A_f) \tag{2.2}$$

where M_s is martensite start, T_o is equilibrium, A_s is austenite start and A_f is austenite finish temperatures.

The Gibbs free energy equal zero at T_o equilibrium temperature, the Gibbs free energy given in the following equation [22] as;

$$\Delta G = \Delta H - T\Delta S \tag{2.3}$$

Where (ΔH) enthalpy change, (ΔG) is Gibbs free energy change, and (ΔS) entropy change [23].

Enthalpy is definite as a quantity of thermodynamic corresponding to the complete heat content of the system. It is the product of pressure and volumeplus internal energy of the system [29].

$$H = PV + E \tag{2.4}$$

However, entropy could be amount of thermodynamic is representative the inaccessibility of a frameworks thermal energy for transformation into mechanical work, it is often interpreted as the degree of disorder within the framework. Entropy alter amounts amid martensitic transformations can be found from the enthalpy value divided by equilibrium temperature T_o.

$$\Delta S_{M\to A} = \frac{\Delta H_{M\to A}}{T_o} \tag{2.5}$$

2.9. Composition and Structure

The structural variation within the martensitic transformations this variation occurs and created by the cooperative motion of all atoms as seen in Figure 2.11. Gained the structure of DO_3 is by stacking the planes B_1 and A_1 as presented in Figure 2.11 within the order B_1A_1, even though the structure of B_2 is accommodated in the structure of DO_3 by taking into consideration the similar planes, however together with lattice parameter $a_0/2$. If the ordering is neglected there are both of these lattices are cubic. The structure of a high-temperature phase change from BCC to more complex structure variation with a low-temperature phase which may have as numerous as 18 atomic layers to characterize the unit cell. This complication of crystal structure makes it troublesome to characterize the relative developments of atoms, frequently depicted as rearranging and shear may be the greatest quantity leading side in martensite transformation involving an individual crystallographic relationship amid the low-temperature phase and high-temperature phase, are bisection coherent interface which permits a fast growth instrument to operate the martensitic transformation including a straightforward shear combined with uniaxial tension or compression normal to the propensity plane, the plane of lattice on which they are shaped the martensite plates appear two diverse substructure to accommodate the shear of the transformation, these are inside twined and inside slipped substructures [4].

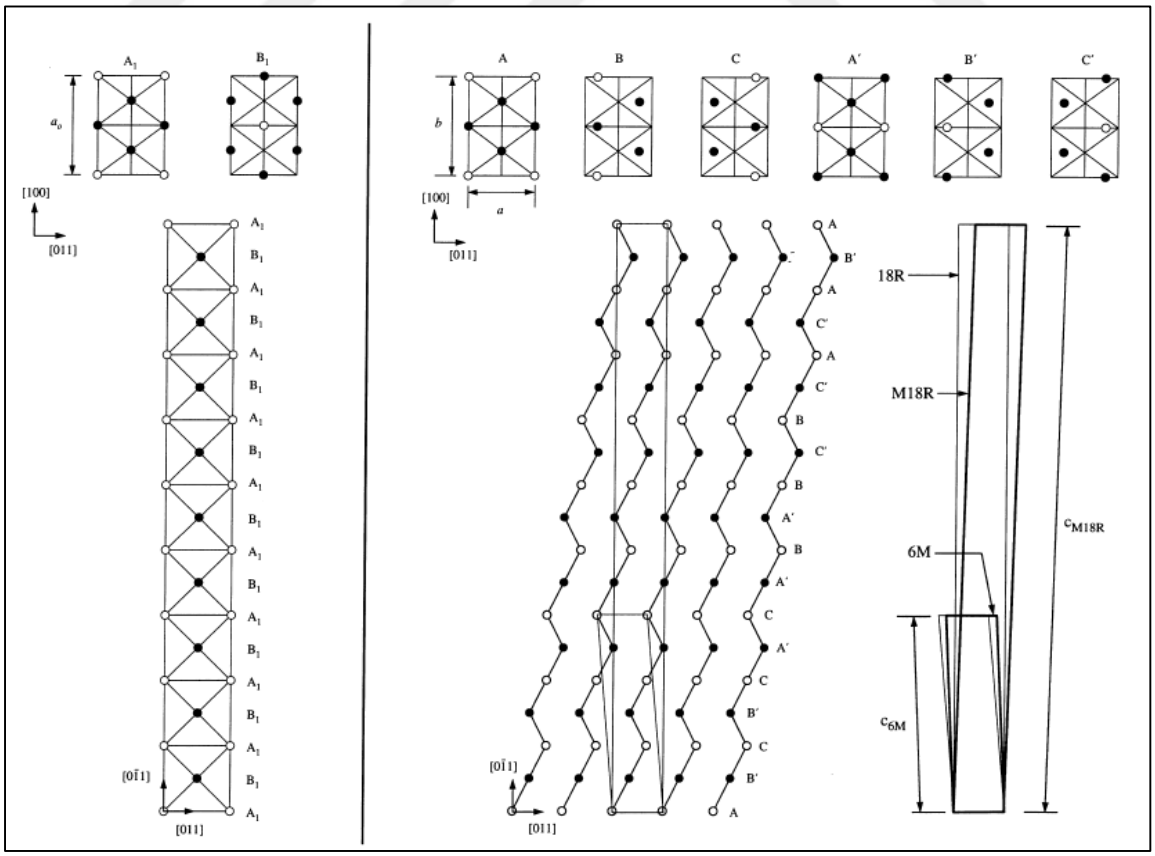

Figure 2.11. The structure variations in martensitic transformations [24].

3. CLASSIFICATION AND APPLICATIONS OF SMAS

Shape memory alloys consisting of different metal elements are generally classified according to the main (the highest percentage) constituting element or binary elements in the SMA systems. SMAs are choosen to be used in applications depending on their demanded properties, costs, processability, functionality, biocompatibility etc.

3.1. Classification of SMAs

Generally, metallic material shape memory alloys can be categorized into six types of alloys that demonstrate shape memory effect in a binary system with addition another element; NiTi-based, Ag-based, Cu-based, Au-based, Co-based alloys and Fe-based. Each of them has a special property of SME and they can modify the properties by changing the composition and by adding or creating ternary and quaternary alloy and changing the ratio of composition [25]. But there are three basses that are rife and have good SME properties for example NiTi-based, Fe-based and Cu-based SMAs.

3.1.1. Copper Based Shape Memory Alloys

Growth of Cu based SMAs has reduced many problems of the NiTi alloys [4]. The copper-based SMAs offer benefits and extending of applications due to their relatively low costs, ease of fabrication, high electrical and thermal conductivity. Fabrication of copper-based memory alloys is made simply by melting the pure raw materials, however, melting loss of volatile elements must be taken into account in the fabrication process and certain alloy composition is essentially required to control transformation temperatures. Cu-based alloys can usually be worked easily more than NiTi alloys although machining is still not as easy as commercial copper alloys and the Cu-based SMAs have a lower manufacturing cost according to Ni–Ti [25, 26]. Cu-based SMAs have three binary alloys (Cu-Sn, Cu-Al and Cu-Zn) as they are shown in the Cu-based SMAs diagram [22] given in Figure 3.1. Diagram of Cu-based shape memory alloys [22]. To modify and improve the good properties of binary SMAs they are produced as ternary and quaternary SMAs by addition of one or more extra additive elements.

The Cu–Al binary alloy systems drive researchers to give obvious attention to these SMAs within the SMA studies. The Cu–Al-based SMAs have high flexible anisotropy primary to low mechanical properties, the short cycle life, and weak intercrystalline failure. In later a long time, numerous researches have been carried out to organize to progress the propertiesof Cu–Al systems by addition extra components such as Ni, Be, and Mn [22, 23].

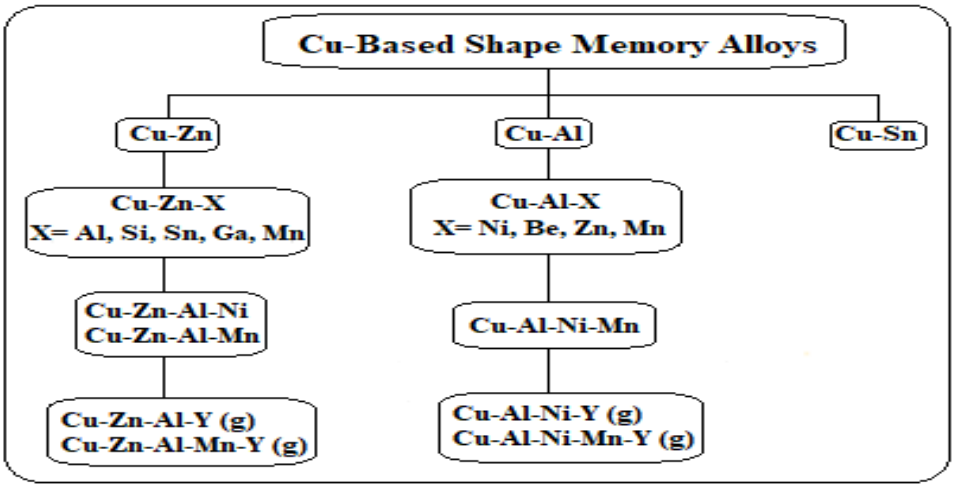

Figure 3.1. Diagram of Cu-based shape memory alloys [22].

3.1.2. Nickel – Titanium Alloys

The NiTi SMA was first discovered in 1962s and that time named NiTinol. It is (NiTi) a classic shape memory alloy in the terms of heat recoverability (8%) [4, 9]. The temperature that is necessary for the phase change to happen thus leads the memory effect to take place can be adjusted from -200 ºC to 100 ºC by the amount of nickel and titanium around the equiatomic ratio of 55 wt.% Ni and 45 wt.% Ti and by addition of other elements. However, sensitivity to slight composition changes makes the transformation temperature extremely difficult to control. This sensitivity is reduced by the addition of copper into NiTi. The fabrication and melting of Titanium–Nickel, and presentation of conventional titanium alloy manufacture are costly because titanium can easily oxidate [27].

3.1.3. Iron-Based Shape Memory Alloys

The third type of fundamental based SMAs is Iron-based shape memory alloys and it was found in 1982, there are two divergent sets of iron-based SMAs[6]. The primary set holds alloys like Fe–Ni–Co, Fe–Pt and Fe–Pd, which illustration the ordinary characteristics of thermoelastic martensitic transformations comparable to NiTi, with a contract warm hysteresis. In any case, despite widespread thinks about, no pseudoelasticity at room temperature has been detailed with Fe–Pt or Fe–Pd and the last set is a set of alloys like Fe–Ni–C and Fe– Mn–Si. The Fe–Mn–Si SMAs have gotten extensive consideration over the past three decades due to extraordinary workability and with a recovery strain of over 5% and a fracture tensile strain of over 8%. as SME in an alloy Fe–Mn–Si alloy. Iron-based SMAs with preferable SME properties have been growing during the past years. It is presumed that this headway will be to lowering the price of these materials and to create them much more economical for applications in civil engineering [28].

3.2. Applications of SMAs

In modern life SMA based smart systems are needed because SMAs is a branch of smart material that is very useful for this purpose and their applications are increasing day by day in many fields for instance automotive, aerospace, robotic and biomedical. The pie chart given in Figure 3.2 shows the patent area of SMAs between 1990-2013.

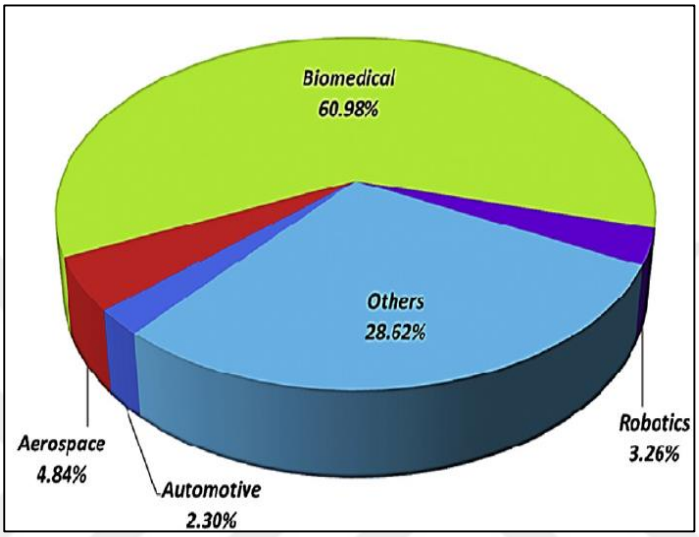

Figure 3.2. Pie chart showing the patent area of SMAs during 1990-2013 [25].

3.2.1. Automotive Applications

In contemporary automobiles, the amount of actuators and sensors are growing greatly by reason of the request for safer, extra relaxed automobiles, the automotive actuators can be for the most part partitioned into three categories; low power actuators for bodywork capacities, high power vehicle actuators controland high-frequency motor actuators control, SMA actuators are most beneficial for the first class and workable for the second class. In any case, SMAs are fewer favorite for the third class due to the low operative frequency and thin bandwidth. Recently, the newly developed SMAs, like NiTi film and magnetic SMAs (MSMAs), have grown the operational frequency up to 2 kHz, but not extend using due it is much slower than other requirements high-frequency actuators [29]. Figure 3.3 illustrates some SMAs application temperature ranges using in automotive purpose and a SMA actuators diagram are given in Figure 3.4.

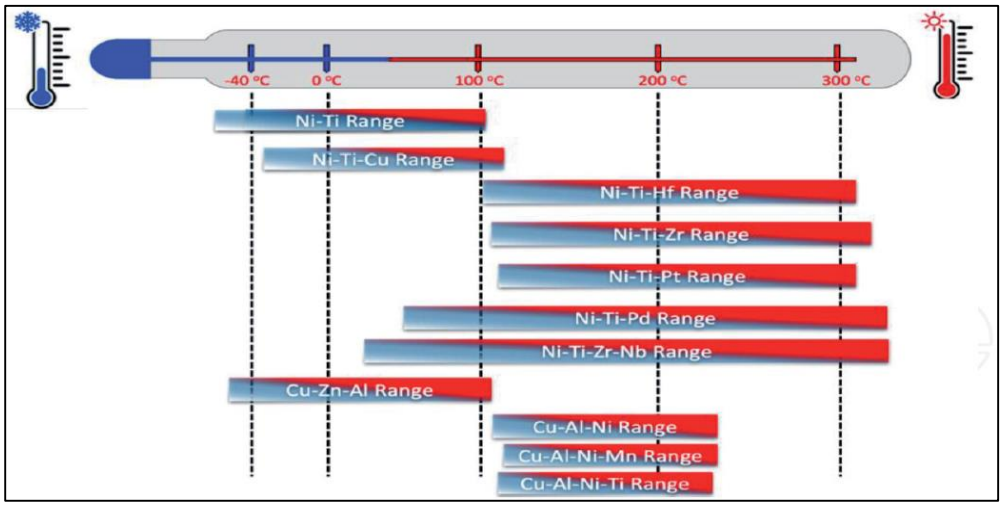

Figure 3.3. Range operating temperature and the transformation temperatures for automobiles applications [15].

Nowadays shape memory alloy actuators are used in an increasing variety of applications due to silent operation, smooth and compact size [30].

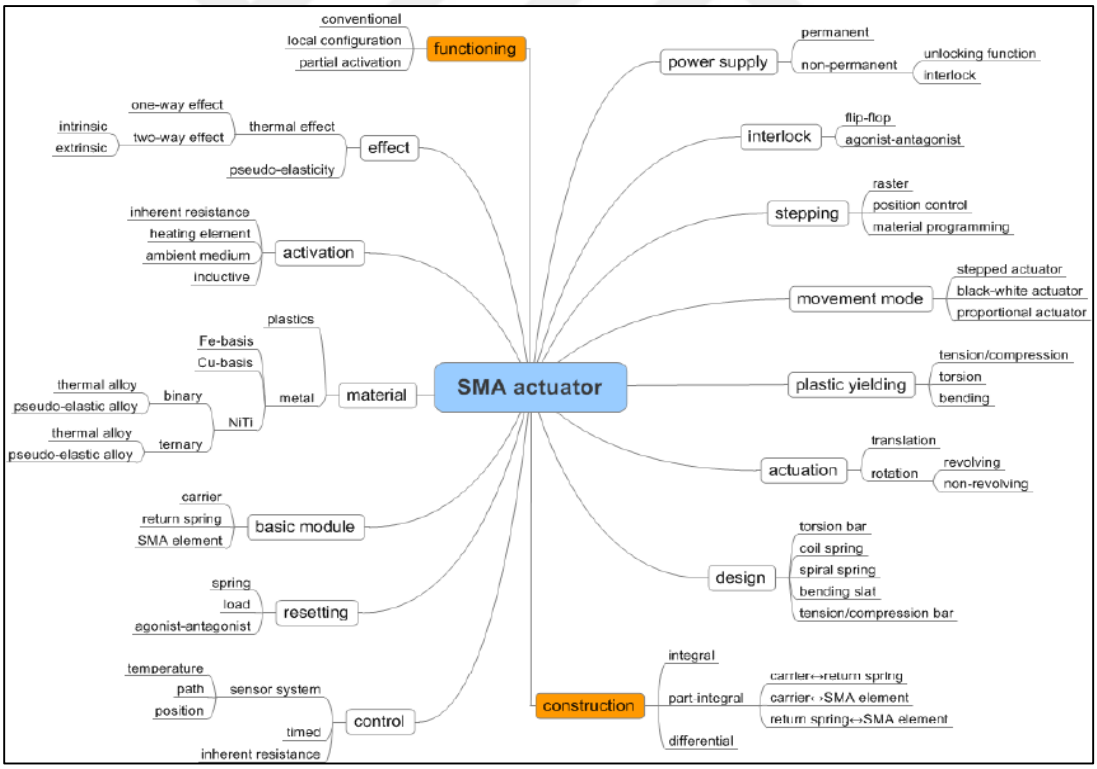

Figure 3.4. SMA actuators diagram [31].

3.2.2. Aerospace Applications

In applications of aerospace systems and structural configurations of the smart wing program with Sea Force System demonstration and the Smart Aircraft SMAs are used as smart

materials due to planned to develop and exhibit the use of active materials to optimize the presentation of lifting bodies. In every application for aerospace, the SME is utilized to supply actuation by shape recovery, and the recovery happens at non-zero stress. The industry of aviation uses shape-memory alloys that reduce noise in engine aircraft's as presented in Figure 3.5.

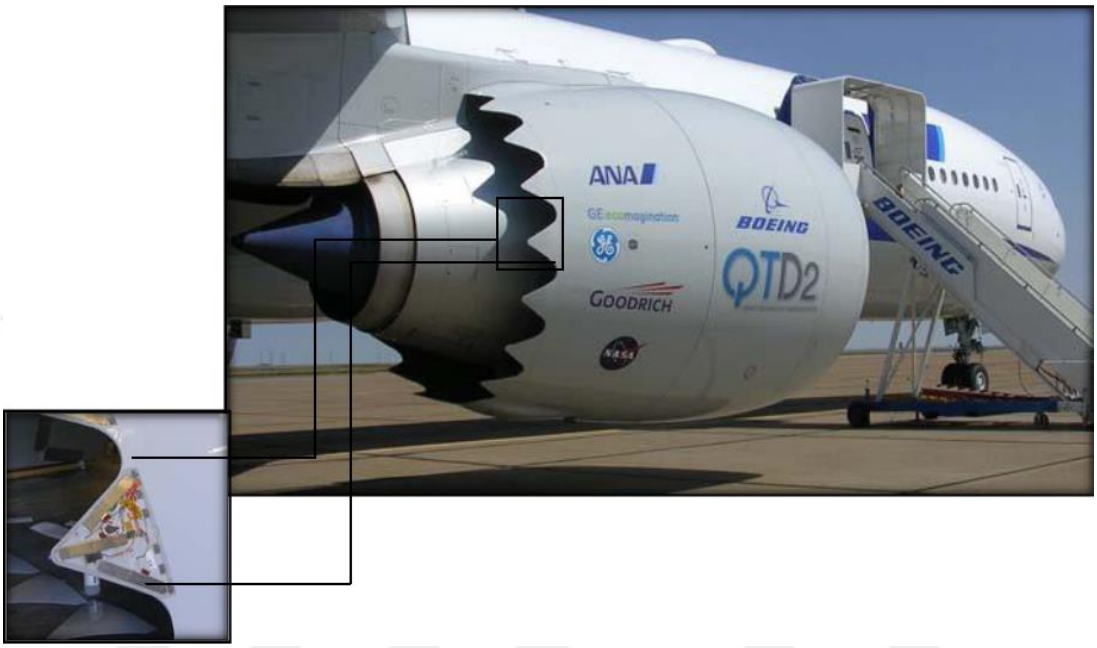

Figure 3.5. An application of SMAs to reduce engine sound in an airplane [32].

3.2.3. Robotic Applications

SMAs have been utilized in a different kind of marketable robotic frameworks and in robotic applications as micro-actuators or synthetic muscles nowadays. The main factors to be considered are; shape (strip/diaphragm, wire/spring) of the actuator, the force required for deforming the actuator, cooling and heating method adopted, sensors combined to measure the parameters like temperature/force/position/temperature, and type of control arrangement implemented. The greatest SMA robotic applications are naturally motivated biomechanics and broadly used in biomedical ranges but are moreover utilized broadly in other areas as well [25, 33]. To grow the intelligence of the integrated system, miniaturization of the hardware boards and expand the performance, numerous practical issues have been underlined and the necessity to be resolved such as small strain output, minute electrical connection for (micro-robots), low electrical resistance, control subjects, and very low efficiency. Still, several of these subjects have been tackled by choosing appropriate modeling procedures, control systems, and response sensors. As an example, the feedback control resistance is perfect for micro-robots as it eliminates the need for additional sensors, while with limited correctness. Figure 3.6 shows some applications of SMAs in the robotic aspect [33].

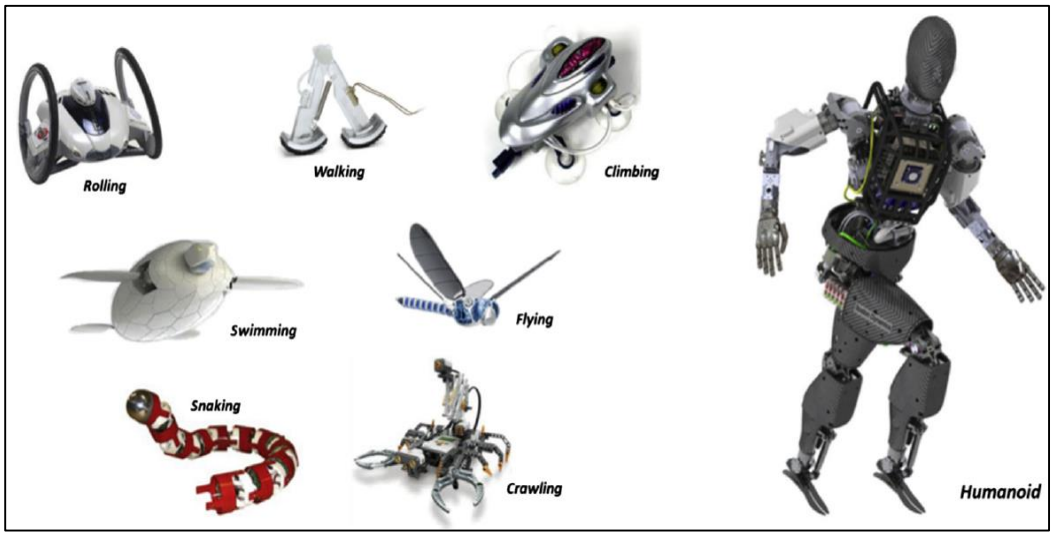

Figure 3.6. Some applications of SMAs using in robotics [25].

3.2.4. Biomedical Applications

Discovering of the SME in nitinolNiTi in 1962 by Buehler et al., it was very important for use in medical applications and not a bad defect and bad reaction on the human body especially at that time, they used for dentistry and a few a long time afterward the first superelastic braces produced from a NiTi alloy were presented by Andreasen in 1971 [10]. Several unique surgical devices have been advanced based on SMA to be important advance into biomedical field afterward its overview in minimally invasive surgery (MIS) [34] and more biomedical requests are growth and presented into the marketplace after the agreement of the Mitek surgical product (i.e. Mitek Anchor) for orthopedic surgery by US Food and Drug Administration (FDA) in 1989. The most important alloy in SMAs for bio medical application is NiTi alloys because it has unique excellent behavior due to bio-compatible [35], non-magnetic [11] high resistance for corrosion [36, 37] properties, which duplicate those of human bones and tissues [38] and it is possible with a change in human body temperature. General using in the medical field is given in Figure 3.7.

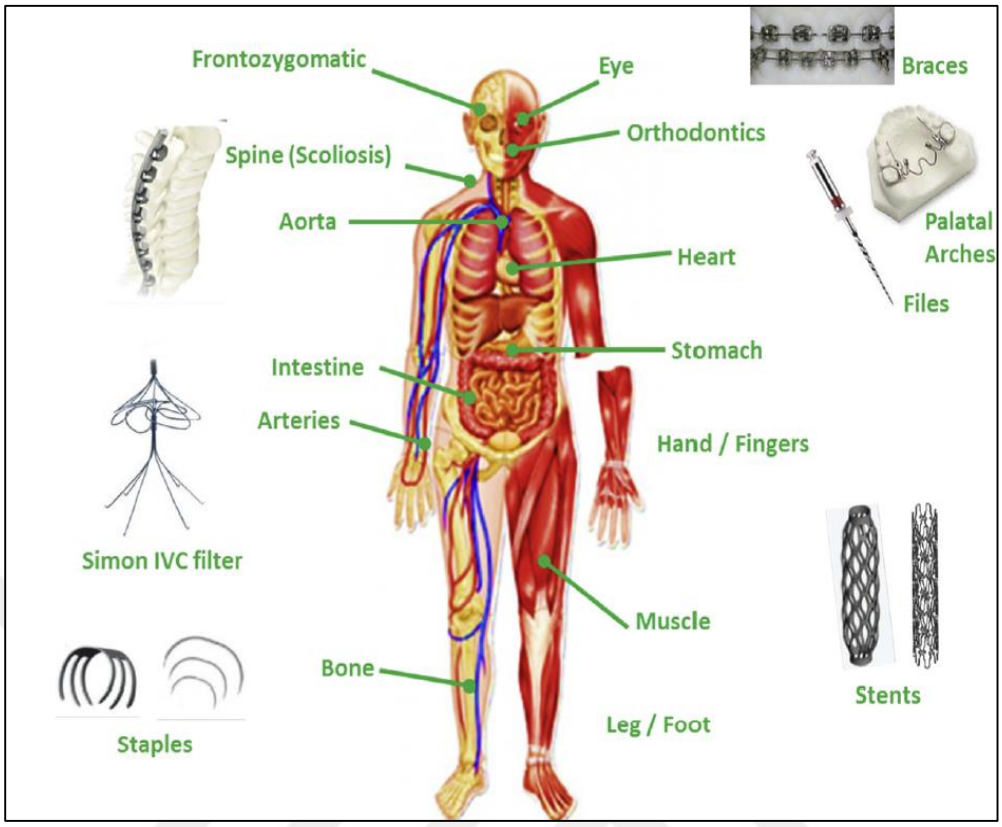

Figure 3.7. SMAs using in different parts of the human body [25].

4. MATERIAL AND METHOD

In this section the methods and details of both the fabrication steps of the ternary and quaternary Cu-based shape memory alloys prepared in this thesis work and the experimental characterization measurements conducted to reveal the fabricated alloys'; chemical compositions, thermal (to observe heat induced reversible martensitic phase transitions which indicate SME property), and structural (crystallography and surface morphology of the alloys in martensite phase) properties.

4.1. Materials

In this thesis, we prepared set four (one ternary and three quaternary) Cu-based shape memory alloys with different and new compositions of Cu–18.73Al–21.06Be–0.13Mn (at.%), Cu–12.9Al–22.73Be-0.37Mn (at.%), Cu-17.33Al-4.74Fe-2.08Mn (at.%) Cu-20.82Al-3.53Fe (at.%) and named as F2, F1, H2 and H1, respectively. To yield the alloys at first the powders of high impurity (99.99%) beryllium, iron, aluminium, manganese, and copper, elements were measured according to their indicated rates and after that mixed for micro homogenization. After then the measured samples of powder mixtures were pressured by using a compressing machine to get them into pellet forms. Then these pellets were melted under argon atmosphere by using an Edmund Buehler model arc melting machine and cast as-cast ingots. These ingots were cut as small pieces (20-45 mg and 2x3x4 mm). Then these small alloy samples were put in a high-temperature oven at 900 ºC for 1 hour for homogenization and right after they were quenched in iced-brine water media to form β1' martensite phase. To detect martensite transformation, alloy samples were tested by a Shimadzu DSC-60A model differential scanning calorimeter (DSC) at different heating/cooling rates of 35, 25, 15 and 5 ˚C/min. To investigate high-temperature behavior of the alloy samples measurements were performed from room temperature to 900 ºC by using a Shimadzu DTG-60AH model differential thermal analysis (DTA) instrument at 45 and 25 ˚C/min of heating/cooling rates. The X-Ray analysis was made at room temperature by using a Rigaku RadB-DMAX II diffractometer with CuKα type X-ray radiation (λ=0.15406 nm) and also optical micrographs Samsung Model XJP-6A/SDC-313 were taken at room temperature.

4.2. EDX Analysis

Energy dispersive X-ray is one of the methods that is an analytical technique used for chemical characterization of a sample or the elemental analysis. As a kind of spectroscopy, it depends on the realization of sample collaborations between matter and electromagnetic radiation, in this process X-ray energies through the material. In the beginning, the inner shells of

the material's atoms knockout by high energy beam to obtain the electrons on the shells of the material. The high energy makes excitation the electron to be knocked-off to a higher energy level, until now this is the first step of the procedure. The second step of the procedure the X-ray to be produced starts when the hitted electron leaves a positive hole as a mark behind and that makes the negative electron from higher energy level shells to be involved and instantly an electron jumps to fill this hole. Jumping from a higher energy level to a lower one means that there is some additional energy that should be free, this releasing comes in the form of some electromagnetic waves or more specifically X-ray (as shown in Figure 4.1). Each element got a different number of electrons and that makes them different in the production of X-ray. A classical EDX spectrum is given in (Figure 4.2) [39].

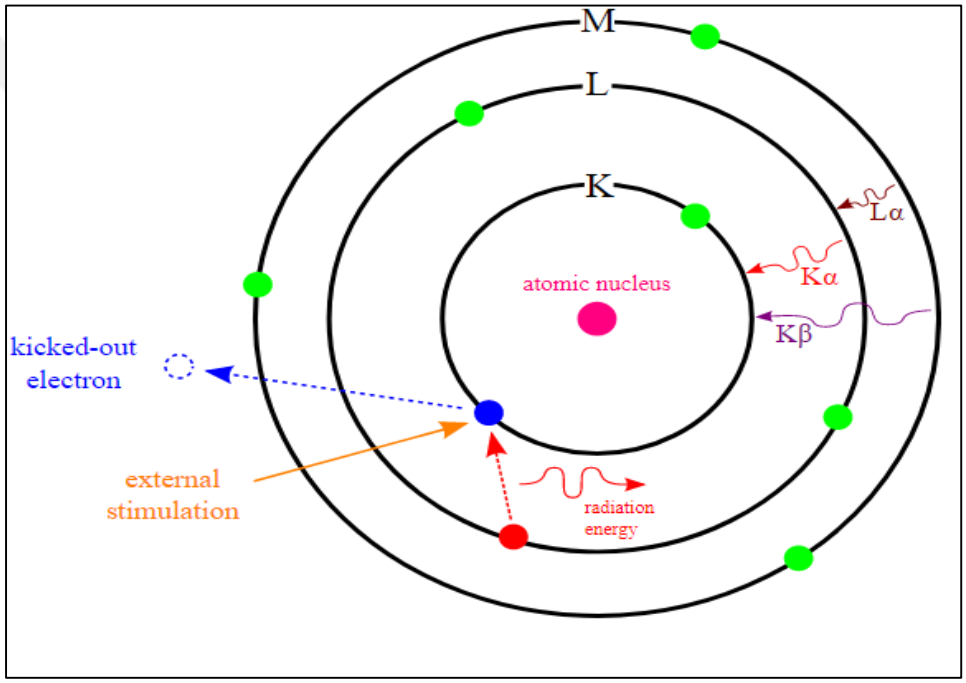

Figure 4.1. X-ray procedure: a) The energy transferred to the atomic electron hits it taking off after a hole, b) Its position is occupied by alternative electron from a higher energy shell and the typical X-ray is released [39].

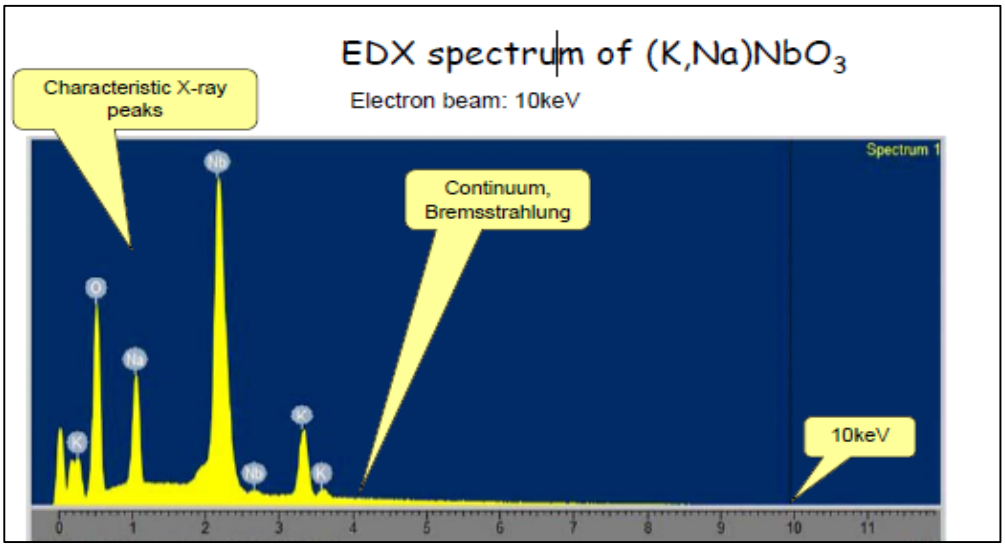

Figure 4.2. Characteristic EDX spectrum: The x-axis shows the energy of the X-rays and y-axis illustrations the numeral of counts [39].

4.3. X-RAY Analysis

X-ray diffraction is a method that is commonly using, nowadays for knowing atomic spacing and the learning of crystal structures. The mean idea of X-ray diffraction is based on the useful interference of crystalline samples and monochromatic X-rays. These X-rays are obtained by the components of those parts; filtered to yield monochromatic radiation,a cathode ray tube, collimated to concentrate, and directed toward the sample. The X-ray production is implemented by heating a filament, the metal with a high melting point, so that it must create an electron from this metal in a cathode tube, is increasing enough heat to the filament at that point electrons will start to move because they have enough energy to elude from the atoms outer shell. After this process produced electrons have to be accelerated to the target direction or a directed point by put on a high voltage and bombarding the target material by electrons as presented in Figure 4.3 [40].

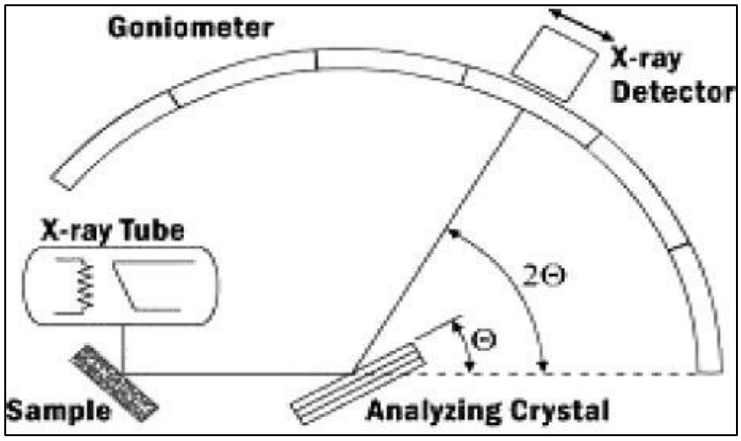

Figure 4.3. Diagram of a diffractometer system [40].

The interaction between incident beams with the sample interference must be satisfied giving to Bragg's law given as below;

$$n\,\lambda \;=\; 2\,d\,sin\,\theta \tag{4.1}$$

where λ is the wavelength of the X-rays, n is an integer, θ is the diffraction angle d is interplanar spacing generating of the diffraction [41]. To calculate the lattice spacing in a crystalline sample and the angle diffraction of incident the wavelength of X-ray we can using Bragg's law (Figure 4.4). While electrons have sufficient energy to eject internal shell electrons of the target material, characteristic X-ray spectra are created. These spectra include of a few components, the rifest being Kα, Kβ, and Kγ.

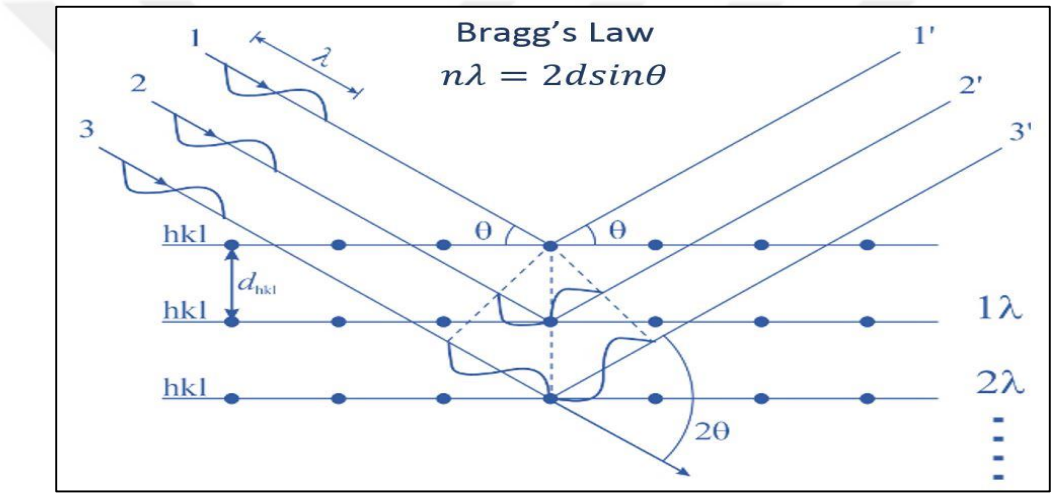

Figure 4.4. Bragg's law and diffraction of X-ray on the planes of the target material [42].

Kα involves in part of $K\alpha_1$ and $K\alpha_2$, $K\alpha_1$ encompasses a small shorter wavelength and two fold the intensity of $K\alpha_2$. The specific wavelengths are typical of the target material (Cu, Mo, Fe, Cr). filtering, by foils or crystal monochromators, is needed to yield monochromatic X-rays necessary for diffraction. $K\alpha_2$ and $K\alpha_1$ are necessarily close in wavelength such that a weighted average of the two is used. Copper is the most popular target material for single-crystal diffraction, with CuKα radiation (λ =1.5418 Å). These X-rays are collimated and directed onto the sample. As the detector and sample are turned, then recorded of the reflected X-rays intensity, the incident of X-rays impinging geometry of the sample satisfies Bragg's law, at that point constructive interference happens and a peak in intensity appears [40].

4.4. Optical Microscopy

The optical micrograph is one of the visual analysis tools used to investigate the grain boundaries and these boundaries govern transport properties and related to device performance on the atomic rearrangement at an element or alloy grain boundaries can be obtained [43]. It consists of a special microscope that has the ability to show inside the grains of the sample. The sample must be prepared for the analysis to be occupied. When the sample is magnified enough so inside grains can be clearly seen with a high-quality camera, the picture of the sample will be taken so that to be analyzed later. Preparation of the sample starts with cutting thin slices of the bulk melt, and then its surface should be smoothed and then dropped a gel form material that is used principally for this purpose so that the sample during the measurements to be held well. In shape memory alloys the optical microscopic surface images are normally taken to see the martensite phases formed in these alloys.

4.5. Differential Scanning Calorimeter (DSC) Analyses

DSC is a essential instrument in thermal analysis aspect of material and alloys. It can be used for industrial and scientific research purposes in many fields. It is a method or way to determine the values of transformation temperatures at zero stress. Historically, temperature transitions in materials were first the time studied by the ceramic industry at the beginning of the nineteenth century.DSC could be a thermal analyzing procedure wherein the difference within the quantity of heat flow required to raise the temperature of reference and a sample are calculated as an effect of temperature. Both reference and the test are protected at about the same temperature during the test [9].

Differential scanning calorimeters normally have two sample locations—one for the sample during exploration and the other for a reference sample, which is often an empty crucible or one full with an inert material as presented in Figure 4.5. [9].

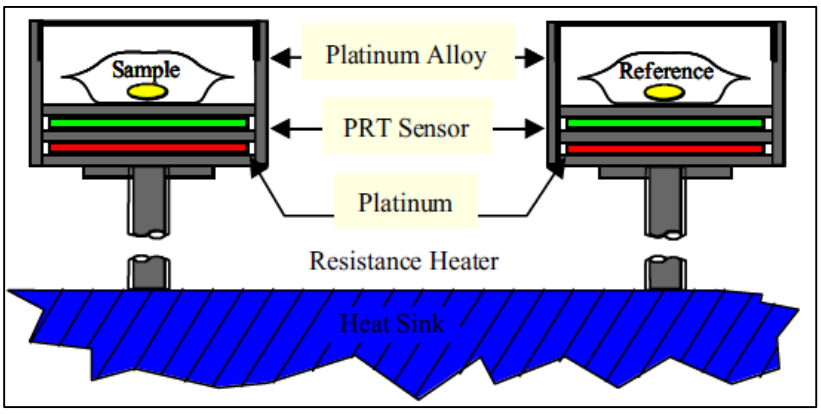

Figure 4.5. Differential scanning calorimeters (DSC) [44].

The DSC instrument produces a plot called thermogram such as presented in Figure 4.6. Between temperature on the X-axis and the amount of heat flow on the Y-axis, heat is given off or absorbed by a sample of the alloy or through the sample in phase transformations. The plot shows both exothermic peaks and endothermic peaks, the endothermic peaks are actions which necessitate energy, because the DSC requires to give additional power to the sample to keep the reference and sample at the equivalent temperature. In a heat flux DSC, these similar occasions cause the sample to absorb heat and be cooler than the furnace, so they point down. The opposite logic applies to exothermic activities when energy is released [9].

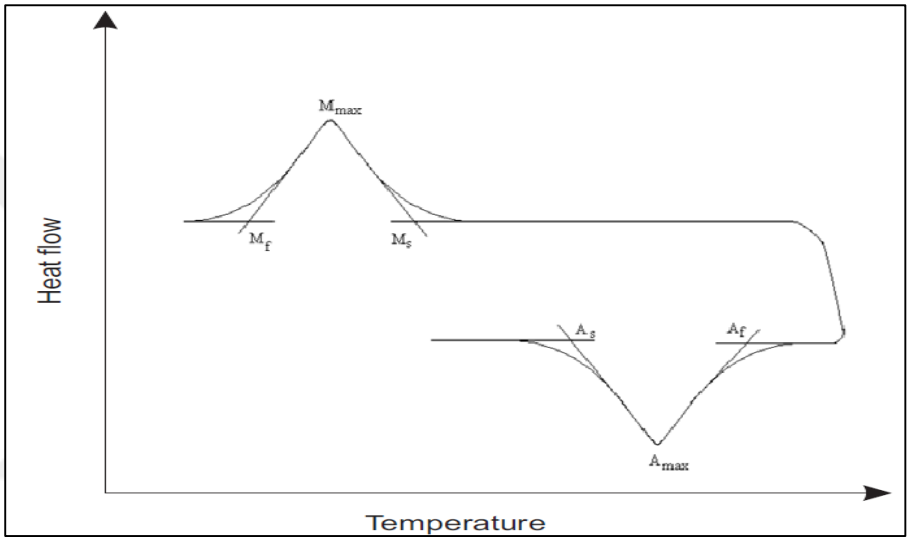

Figure 4.6. A DSC thermogram showing the transformation peaks and temperatures [45].

4.6. TG/DTA Analysis

The thermogravimetry (TG) or differential thermal analysis (DTA) is a thermal analyzing method like DSC. This device does two important thermodynamic analyses at the same time as shown in Figure 4.7. The sample is generally in the solid-state and change on heating includes melting, decomposition, phase transition and sublimation. The investigation of the variety within the mass of a sample on warming is called as thermogravimetric analysis (TG) [46]. Differential thermal analysis (DTA) is another technique used for investigation and associated the temperature of the substance with the temperature of a thermally inert material.

TG estimation mass varieties in a material under test duringheat as a functionalof temperature (or time) in exact atmosphere. Its fundamental procedures incorporate investigation of a material's thermal stability and composition. In Figure 4.7 the peaks on the DTA line indicate an endothermic reaction at nearby 600 ºC and an exothermic reaction about 1000 ºC [46].

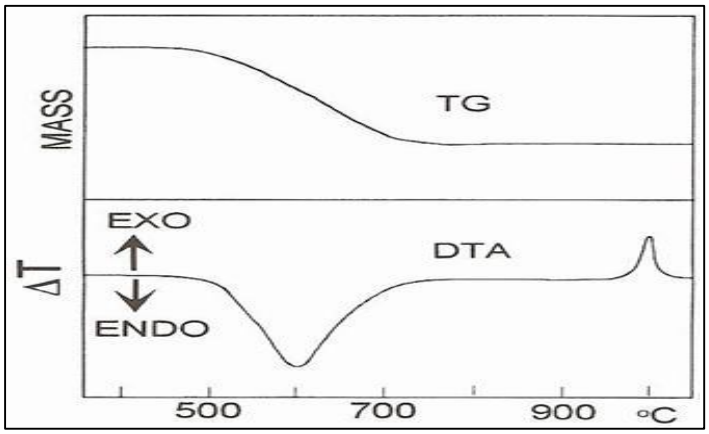

Figure 4.7. TG & DTA curves for $Al_4(Si_4O_{10})(OH)_8$ [47].

5. RESULTS AND DISCUSSION

This section includes the results of the experimental SMA characterization tests conducted on the Cu-based shape memory alloys produced in this thesis work and the interpretation and discussion of these findings.

5.1. Energy Dispersive X-Ray (EDX)

The element percentages (i.e. the atomic ratios; at.%) in the alloys were investigated by using energy dispersive X-ray (EDX) Bruker Model device at room temperature to determine the chemical compositions of each alloy. The copper-rich alloys were named H1, H2, F1, and F2, and their chemical compositions are presented in Table 5.1.

Table 5.1. Electron concentrations and chemical compositions of elements.

Alloy ID	Chemical composition (at.%)					Electron concentration (e/a)
	Cu	Al	Be	Fe	Mn	
F1	64	12.9	22.73	-	0.37	1.489
F2	60.08	18.73	21.06	-	0.13	1.5865
H1	75.65	20.82	-	3.53	-	1.4517
H2	75.85	17.33	-	4.74	2.08	1.4148

One important effective parameter in alloys named electron concentration (e/a) as given in Table 1, it influences on the characteristics of transformation temperature, the percentages of the element in the composition cause to change both transformation temperature and *e/a*. Electron concentration *(e/a)* for Cu-based SMAs should generally be in the range between 1.45 and 1.51. The e/a values give us a prediction about the crystal structure of Cu-based SMAs and in this e/a range the structure can include both types of martensite; $\beta'1(18R)$ and $\gamma'1(2H)$ martensite forms. Here e/a values for both H1 and F1 alloys are in this range, if e/a value is smaller than 1.45 then the structure is dominantly $\beta'1(18R)$ type martensite so this should be in H2 alloy and if it is greater than 1.51 at this time $\gamma'1(2H)$ type martensite becomes the dominant phase [48, 49] which is expected in F2 alloy. In this work, were calculated the electron concentration values of the alloys by the below equation [49] as;

$$\frac{e}{a} = \sum f_i v_i \tag{5.1}$$

where f_i represents each fraction of alloying elements and v_i is the valence numbers of those elements.

5.2. Optical Microscopy Images

The optical micrographs were taken at room temperature by a magnification of 10μm for all samples as shown in Figure 5.1-5.4. On these micrographs, the grains and grain boundaries can be clearly seen. Martensite plates sharply separated by these grain boundaries. Martensite variants with different orientations appear on the surface of the alloys formed as needle-shaped *18R(β1`)* type martensite phase and alongside with them thicker *2H(γ1`)* type martensite forms.

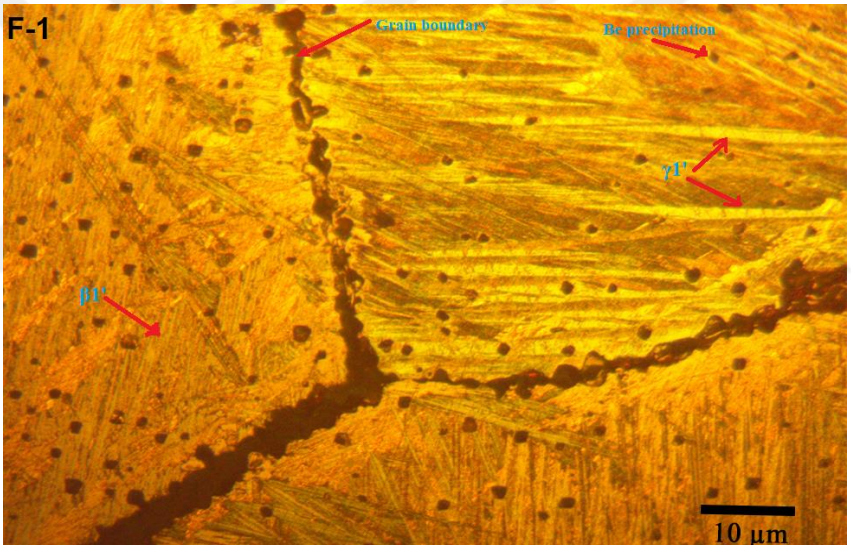

Figure 5.1. Optical micrograph displaying surface of F1 alloy.

On the optical micrograph displaying F1 alloy's surface given in Figure 5.1 the needle-shaped martensite *18R(β1`)* forms together with *2H(γ1`)* martensite forms, grain boundaries and Be precipitation spots can be seen.

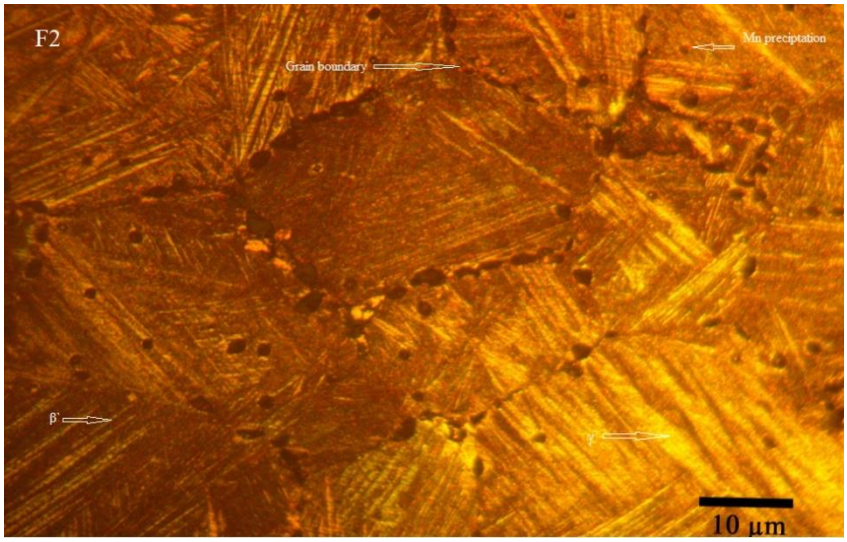

Figure 5.2. Optical micrograph displaying surface of F2 alloy.

The optical micrograph of F2 alloy as presented in Figure 5.2, displays needle-shaped *β1`*martensite phase together with *γ1`* martensite phase, grain boundaries, and Mn precipitations.

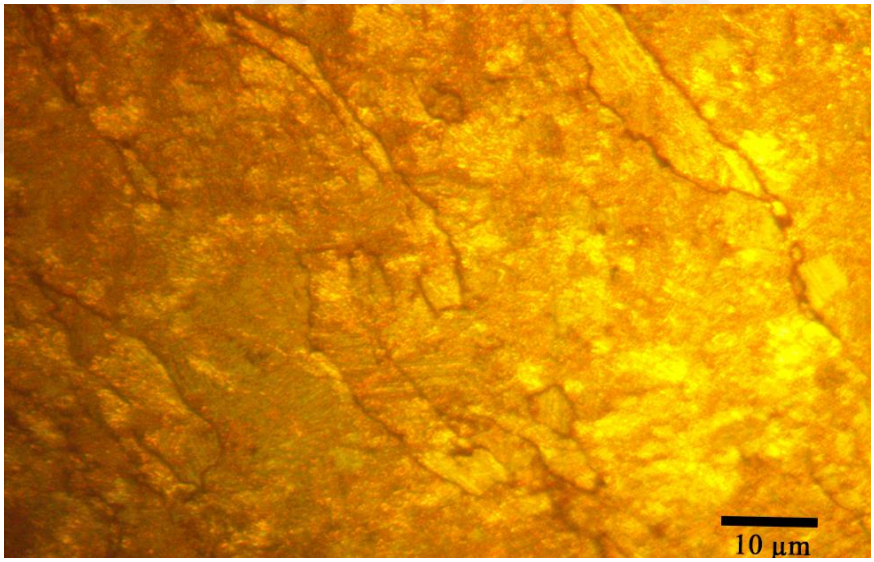

Figure 5.3. Optical micrograph displaying surface of H1 alloy.

On the optical micrograph of H1 alloy as presented in Figure 5.3 there is seen irregular boundaries which may have formed due to Fe effect on Cu-Al alloy base or a melting process ended with an imperfect homogeneity (a melting fault), but at least still both types of martensite forms can fuzzily be discerned.

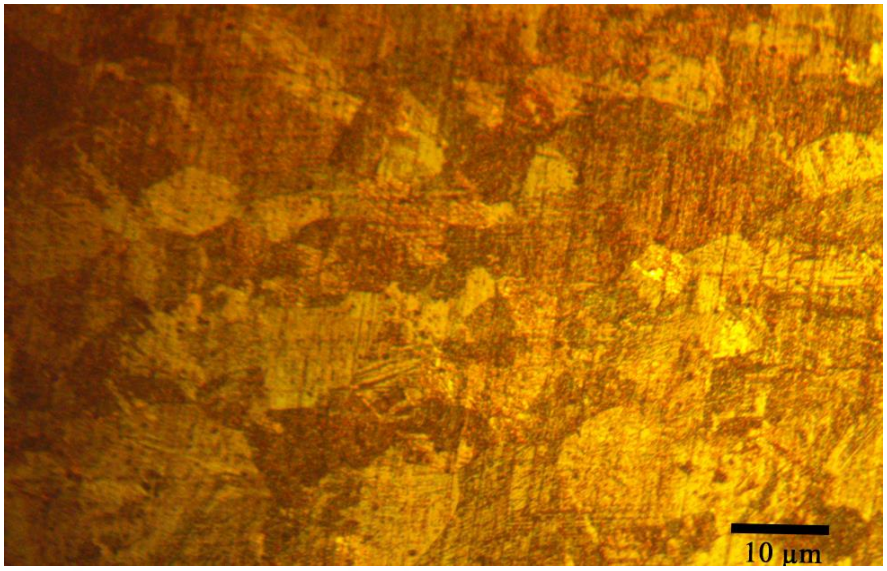

Figure 5.4. Optical micrograph displaying surface of H2 alloy.

According to the optical micrograph of H2 alloy given in Figure 5.4, at this time there can be seen the effect of additive Mn element on CuAlFe alloy base led to form the smallest grains among those of the other alloy samples and also both martensite forms and precipitations.

5.3. Differential Scanning Calorimetry (DSC) Measurements

The results of thermal DSC measurements were taken at various heating/cooling rates for each one of the alloy samples and the obtained DSC curves can be seen in Figures 5.5-5.8. On all of these DSC curves, the downward endothermic peaks on the downward heating parts indicate the phase transformations from martensite to austenite, and conversely on the upward cooling parts of the DSC cycles there exist upward exothermic peaks implying the phase transitions occur from austenite to martensite. There are also some missed or shallow peaks on these curves, especially on the curves of H2 alloy at slow heating cooling rates. This happened due to in consequence of both the slower heating/cooling rates and weaker SME property of H2 alloy.

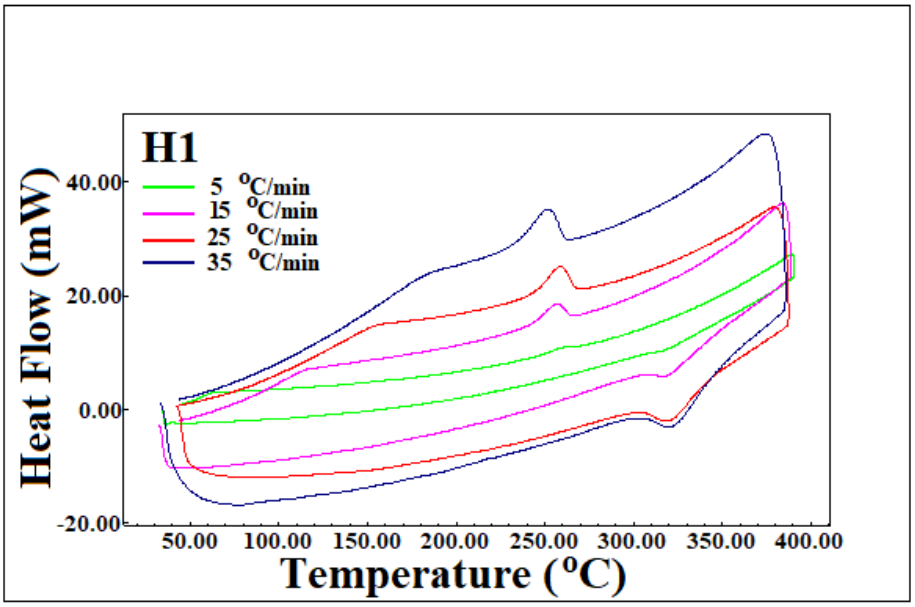

Figure 5.5. DSC curves of H1 alloy at 5, 15, 25 and 35 °C/min of heating/cooling rates.

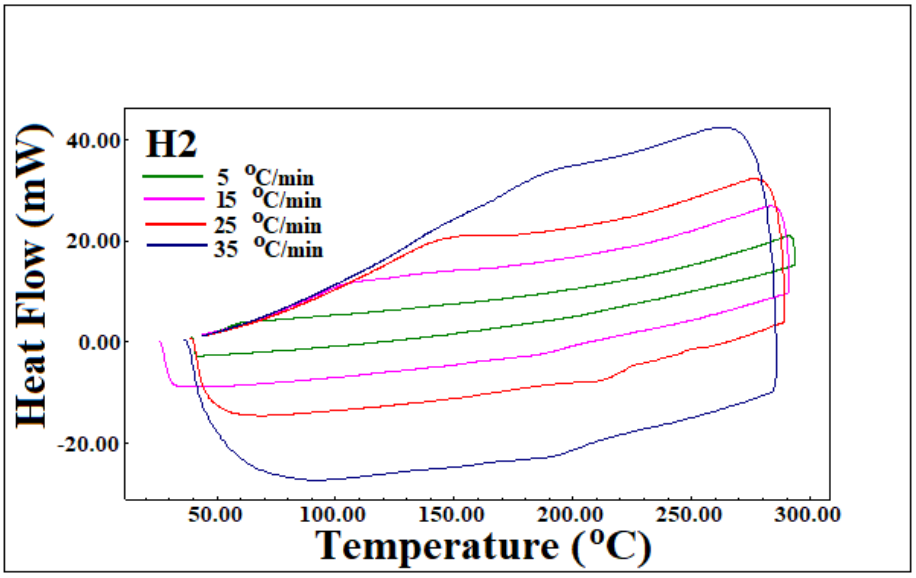

Figure 5.6. DSC curves of H2 alloy at 5, 15, 25 and 35 °C/min of heating/cooling rates.

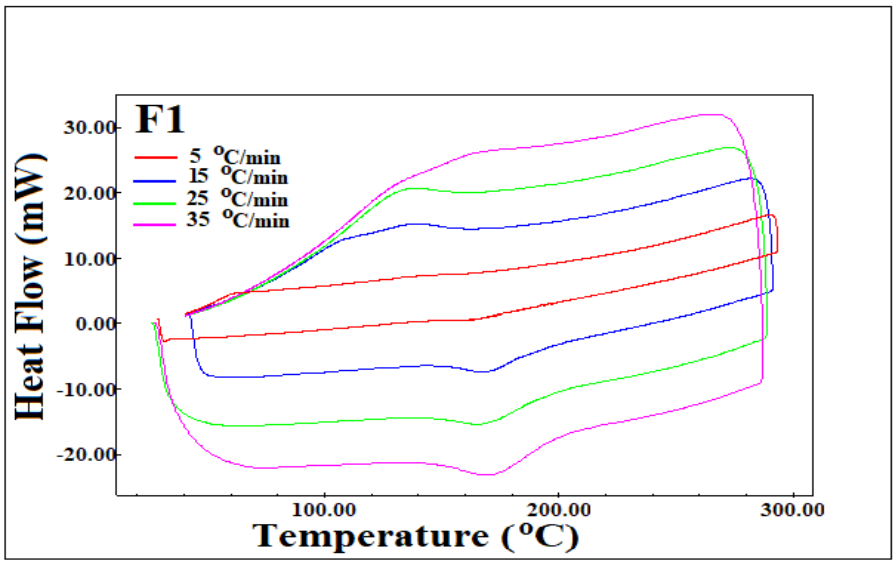

Figure 5.7. DSC curves of F1 alloy at the heating/cooling rates of 35, 25, 15, and 5 ˚C/min.

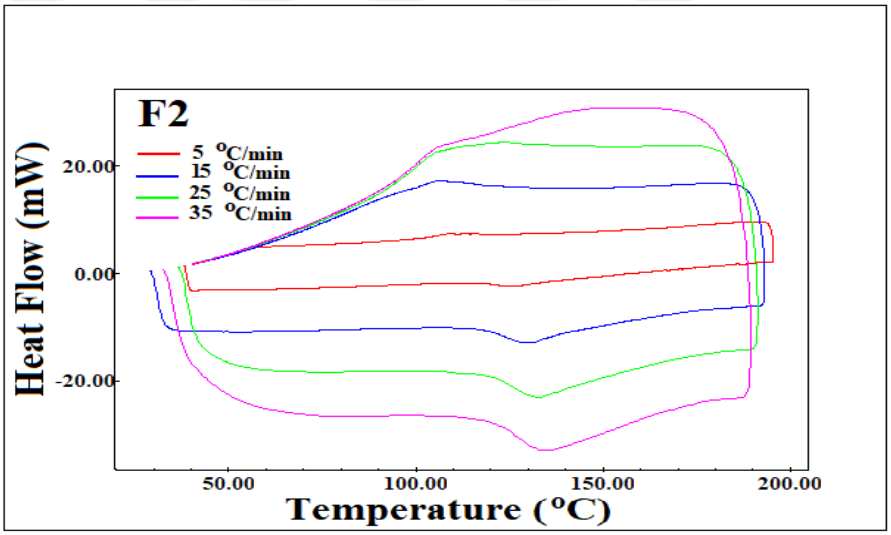

Figure 5.8. DSC curves of F2 alloy at the heating/cooling rates of 35, 25, 15, and 5 ˚C/min.

The values of thermodynamical transformation temperatures of A_s, A_f, M_s, M_f, A_{max} (maximum austenite peak temperature), hysteresis $(A_s\text{-}M_f)$ and enthalpy change (ΔH) parameters for all of the back and forward transformations that obtained by applying the tangent method on these transformation peaks by using DSC thermal analyzer program and the values of other thermodynamic parameters such as equilibrium temperature (T_o) and entropy change (ΔS) were all calculated for each alloy and transformation and given in Table 5.2. According to these DSC curves and values in Table 5.2 it can be said that the martensitic transformation peaks are very sensitive to the alloy element composition and they varied a bit with different heating rates influenced by the heating process. The transformation peaks shape and position at martensite–

austenite transformation peaks changed depending on the heat flow and transformation temperature values.

Table 5.2. The values of transformation temperatures of H1, H2, F1 and F2 alloys at different heating rates with thermodynamic parameters.

Alloy ID	Rate (°C/ min)	As (°C)	A_f (°C)	A_{max} (°C)	Ms (°C)	M_f (°C)	As-M_f (°C)	T_o (°C)	$\Delta H_{M\rightarrow A}$ (J/g)	$\Delta H_{A\rightarrow M}$ (J/g)	$\Delta S_{M\rightarrow A}$ (J/g°C)	$\Delta S_{A\rightarrow M}$ (J/g°C)
H1	5	308.28	326.04	320.84	267.092	253.61	54.67	296.56	2.27	-5.96	0.007654	-0.0201
	15	309.13	346.76	316.25	264.29	244.12	65.01	305.52	3.05	-2.62	0.009982	-0.00858
	25	307.34	337.39	318.33	267.28	243.38	63.96	302.33	4.69	-1.6	0.015512	-0.00529
	35	306.07	340.94	319.7	261.51	234.9	71.17	301.22	6.3	-6.39	0.020914	-0.02121
	Avg.	307.70	337.78	318.78	265.04	244.00	63.70	301.41	4.077	-4.14	0.013516	-0.01379
H2	5	199.33	210.81	205.29								
	15	168	200.7	205.46	160.4	122.73	45.27	180.55	4.7	-2.56	0.026031	-0.01418
	25	202.49	229.36	236.03	180.19	134.64	67.85	204.77	2.37	-2.71	0.011573	-0.01323
	35	172.76	210.81	196.14	199.02	155.09	17.67	204.91	1.27	-1.82	0.0061977	-0.00888
	Avg.	181.08	213.62	212.54	179.87	137.48	43.59	196.74	2.78	-2.36	0.014601	-0.0121
F1	5	160.36	186.06	166.65	156.06	113.83	46.53	171.06	2.17	-6.80	0.012686	-0.03975
	15	152.32	184.19	167.05	155.51	121.08	31.24	169.85	2.42	-6.20	0.014248	-0.0365
	25	146.23	193.31	165.65	153.26	118.27	27.96	173.28	4.99	-5.83	0.028796	-0.03364
	35	148.72	194.64	169.05	184.49	148.21	0.51	189.56	0.96	-5.47	0.005064	-0.02886
	Avg.	151.90	189.55	167.1	162.33	125.34	26.56	175.94	2.635	-6.07	0.015198	-0.03469
F2	5	117.26	124.46	124.86	113.6	101.2	16.06	119.03	2.73	-3.72	0.022935	-0.03125
	15	119.37	141.75	130.12	118.76	100.45	18.92	130.25	1.64	-6.08	0.012591	-0.04668
	25	119.83	151.42	132.84	131	97.26	22.57	141.21	7.32	-7.67	0.051838	-0.05432
	35	120.2	163.21	134.53	117.81	95.51	24.69	140.51	1.2	-8.00	0.00854	-0.05694
	Avg.	119.16	145.21	130.587	120.29	98.605	20.56	132.75	3.22	-6.36	0.023976	-0.0473

By addition a small amount of Mn, the DSC curves indicated that different values of the thermodynamic parameters indicate the effect of adding Mn to ternary alloy Cu-Al-Fe that changed all the thermodynamic parameters of M_s, M_f, A_s, A_f, respectively as they decreased. The low temperature reverses $A \rightarrow M$ martensitic transformations and high-temperature direct martensite $M \rightarrow A$ presented themselves as upward exothermic peaks and down-endothermic, individually for both alloy samples H1 and H2, as these are classic performances of the SMAs.

According to all data in Table 5.2, the characteristic transformation temperatures of H1 alloy have become the highest among those of the other alloys due to the effects of doping Mn, increasing Fe, and decreasing Al contents. However, since the DSC cycle of H2 alloy was taken at slow 5 °C/min of heating/cooling rate as presented in Figure 5.6 the values of M_S, M_f and A_{max}

temperatures for H2 alloy could not be determined due to that austenite to martensite transformation peak did not appear on this DSC cycle of H2 alloy.

The DSC measurements for F2 and F1 alloys were achieved,beginning at room temperature to 200 °Cand 300 °C respectively for both alloys, with different heating/cooling rates of 35, 25, 15, and 5 ºC/min, respectively for each alloy sample as appeared in Figure 5.7 and Figure 5.8.

The DSC results clearly display the martensitic transformation peaks appeared for both of alloy samples. So that, on the cooling and heating parts of these curves there can be seen low temperature reverse A→M martensitic transformations and high-temperature direct martensite M→A as up-exothermic peaks and down-endothermic respectively for both samples, which characterize the SME property and typical behaviors of the SMAs. The endo-peaks on heating parts of these curves in many positions and sizes refer to the $M \rightarrow A$ transformation among of 117.26 ºC to 124.46 ºC and 146.23 ºC to 194.64 ºC and for F2 and F1, respectively and contrariwise exo-peaks on cooling parts the indicating $A \rightarrow M$ transformations placed between 113.6 ºC to 95.51 ºC and 153.26 ºC to 113.83 ºC for F2 and F1, respectively. The characteristic transformation temperatures of A_s, A_f, M_s *and* M_f and some extra kinetic parameters of the samples for example equilibrium temperatures, entropy (ΔS) and enthalpy (ΔH) change were also investigated according to analyses of DSC curves. The values of equilibrium temperature and ΔS parameters were calculated by using equations (2.2 and 2.5). Those A_s, A_f, A_{max}, hysteresis $(A_s\text{-}M_f)$ values conversely increasing with decreased heating/cooling rates for the F1 sample, and hysteresis values directly proportional with heating/cooling rate for the F2 sample.

From Table 5.2, ΔH enthalpy changes spent during the martensite (*M)* to austenite (*A*) and reverse transitions in all of the alloy samples were plotted as shown in Figure 5.9 and Figure 5.10 respectively.

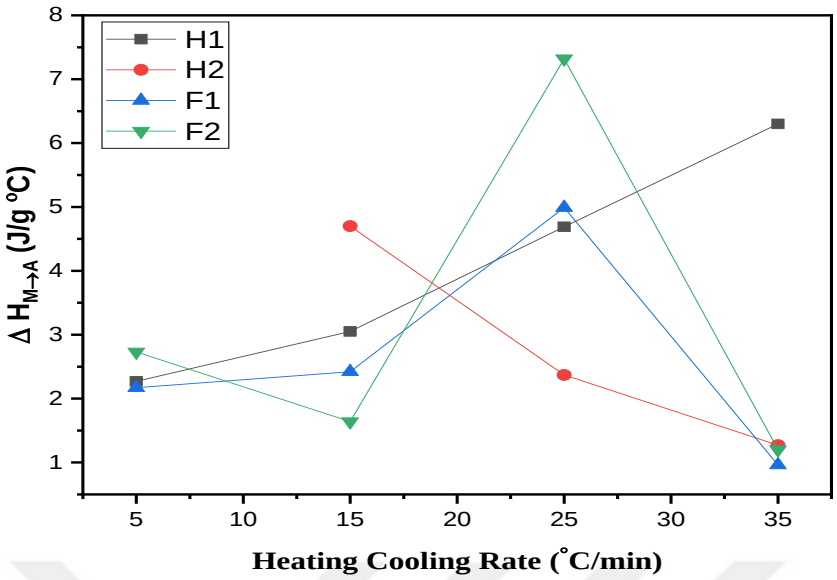

Figure 5.9. Enthalpy change $\Delta H_{M\rightarrow A}$ values changing between H1, H2, F1and F2 alloys with heating/cooling rates.

According to Figure 5.9, the highest value of $\Delta H_{M\rightarrow A}$ belongs to F2 alloy (7.32 J/g °C) at rate 25 °C/min and the lowest value (0.95 J/g °C) for F1 at rate 35 °C/min and $\Delta H_{M\rightarrow A}$ values become approximately equal at a rate of 18 °C/min.

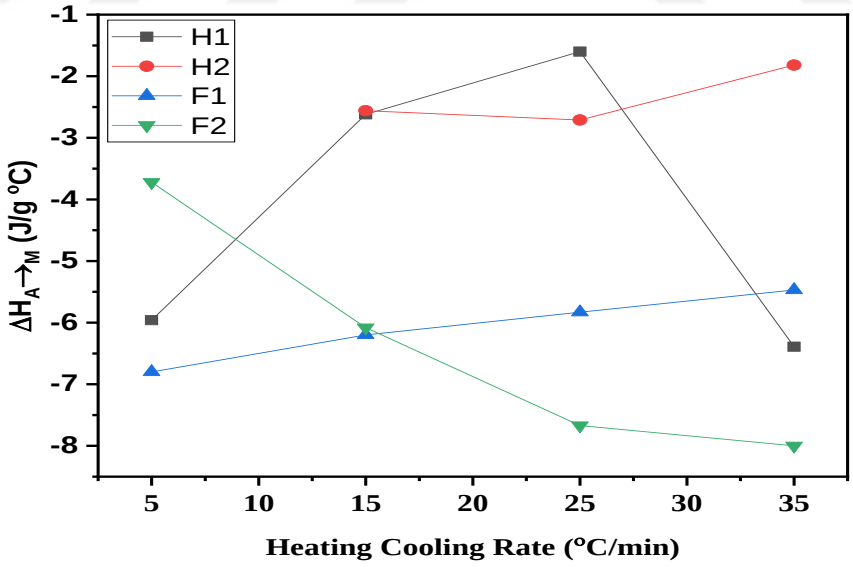

Figure 5.10. Enthalpy change $\Delta H_{A\rightarrow M}$ values changing between H1, H2, F1and F2 alloys with heating/cooling rates.

As seen from the Figure 5.10, the highest value of $\Delta H_{A\rightarrow M}$ belongs to H1 alloy (-1.6 J/g °C) at rate 25 °C/min and its lowest value is (-8 J/g °C) for F2 alloy at rate 35 °C/min and from the

Figure 5.10 have some approximate equality points such as at rate 10 °C/min for H1 and F2 (-4.6 J/g °C), rate 15 °C/min for F1and F2 (-6.5 J/g °C) and (-2.6 J/g °C) for H1and H2.

The variation in both average enthalpy change and average hysteresis values with e/a ratios are presented in Figure 5.11 and Figure 5.12. Those figures show the transformation temperature of the alloys and the relation of electron concentration [50].

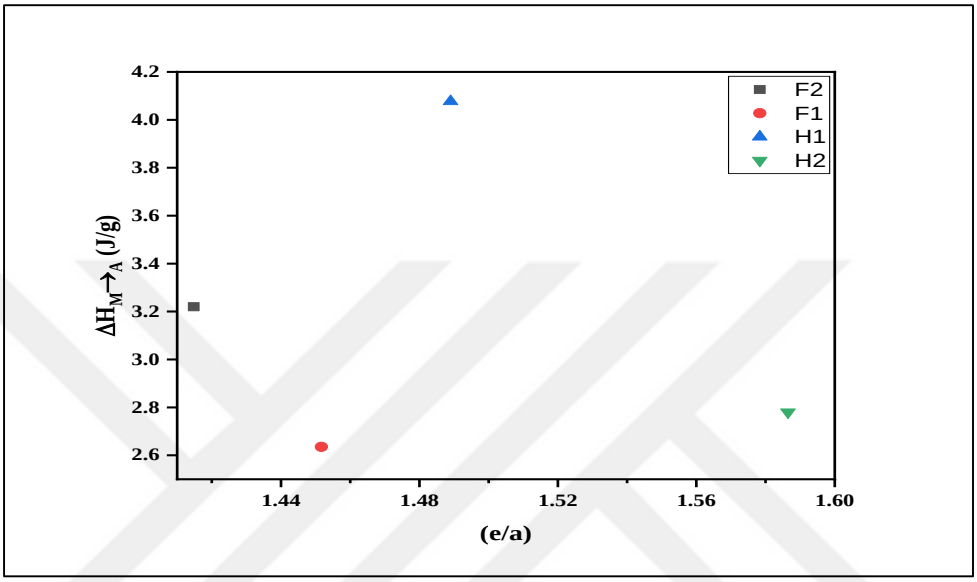

Figure 5.11. The *e/a* ratio changing with average enthalpy change $\Delta H_{M\rightarrow A}$ values for all samples.

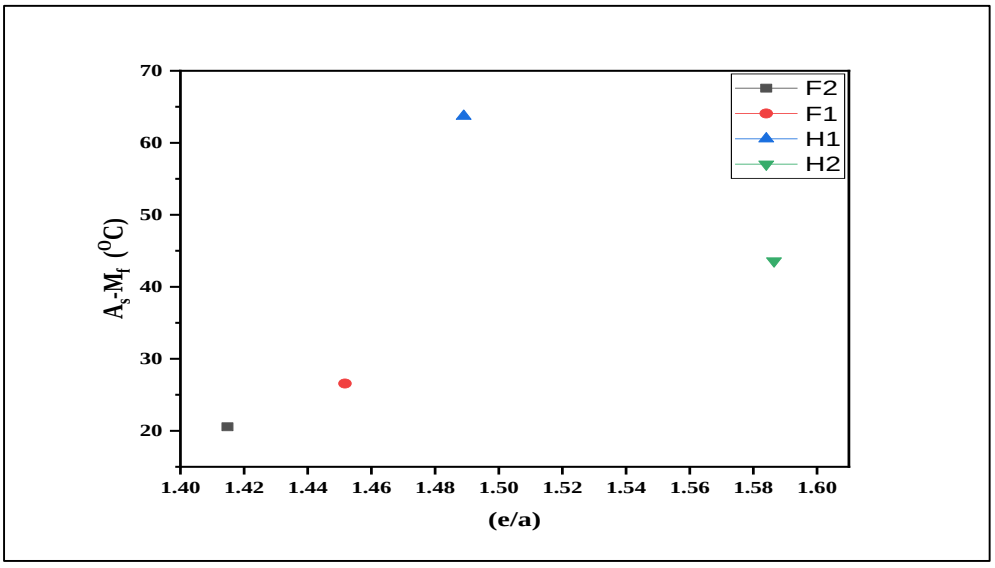

Figure 5.12. The *e/a* ratio changing with average hysteresis values for all samples.

Another important thermodynamic parameter is entropy change. Again by using the data in Table 5.2, the ΔS entropy changes occurred during the direct and reverse martensitic

transformations in all of the alloy samples were plotted as shown in Figure 5.13 and Figure 5.14, respectively. According to Figure 5.13, the highest value of $\Delta S_{M\rightarrow A}$ belongs to F2 alloy (0.051831 J/g °C) at rate 25 °C/min and the minimal value is (0.005164 J/g °C) for F1 at rate 35 °C/min and we noted that all entropy values change with heating/cooling rate.

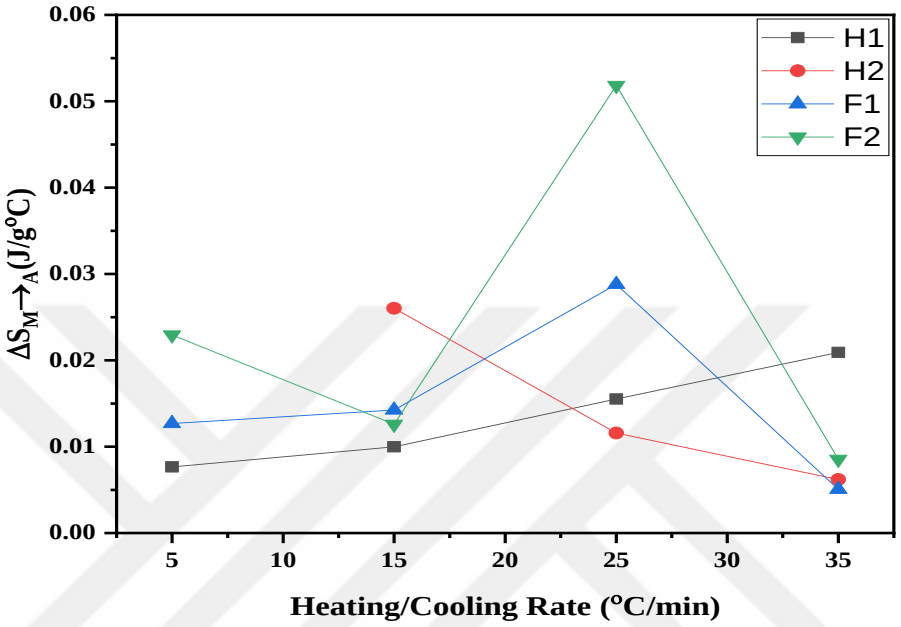

Figure 5.13. Entropy change $\Delta S_{M\rightarrow A}$ values changing between H1, H2, F1and F2 alloys with heating/cooling rates.

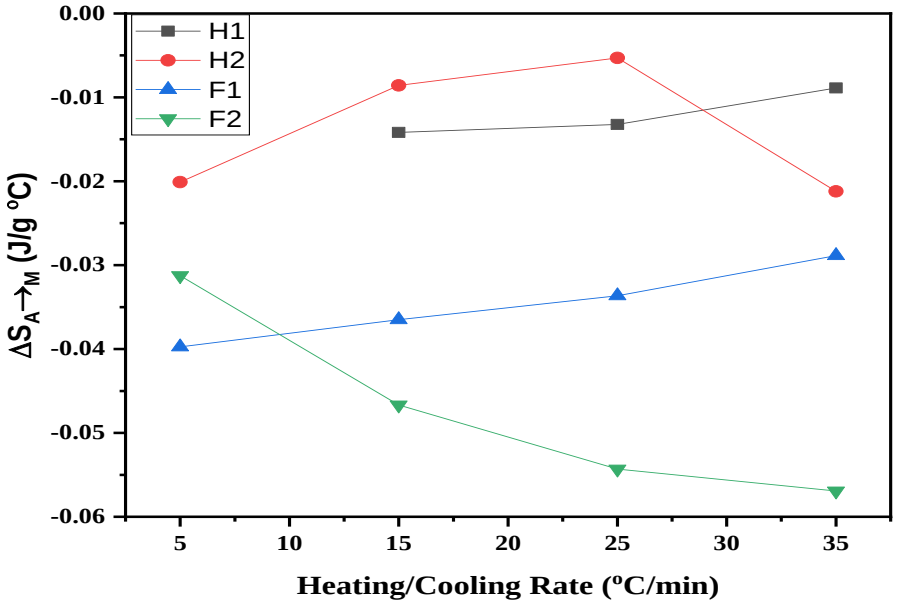

Figure 5.14. Entropy change $\Delta S_{A\rightarrow M}$ values changing between H1, H2, F1and F2 alloys with heating/cooling rates.

In regard to Figure 5.14, the highest value (-0.00888 J/g °C) of entropy change $\Delta S_{A\rightarrow M}$ belongs to H2 alloy at rate 25 °C/min and the lowest value is (-0.05694 J/g °C) for F1 alloy at rate 35 °C/min and we noted to that an approximate equality of $\Delta S_{A\rightarrow M}$ values (to -0.038 J/g °C) for F1 and F2 alloys at rate 10 °C/min and for H1 and H2 alloys at rate 28 °C/min (to -0.013 J/g °C).

5.4. Activation Energy

The activation energy (E_a) is defined as that it is the lowest energy necessary for a chemical reaction to occur or phase transformation in a material (here in shape memory alloys) during heating cooling processes. The values activation energy can be determined from the peak shifts on the DSC curves obtained at different heating rates as shown in Figure 5.15. This important kinetic parameter is the energy required in reverse and direct transformations that occur in the alloy samples and determines the crystallization behaviors of the alloys. Here, in order to evaluate the activation energy values of alloy samples the Kissinger equation [22, 23] is given as below;

$$-\frac{E_a}{R} = \frac{d\left[ln\left(\frac{\phi}{T_m^2}\right)\right]}{d(1/T_m)} \tag{5.1}$$

where; Φ is heating/cooling rate, R is the universal gas constant (R=8.314 J/mol.K), T_m is maximum austenite peak temperature (A_{max}) on DSC curve. The term in the second side of this equation was depicted as plots of $ln(\Phi/T_m^2)$ versus $1000/T_m$ for each alloy sample. For all of the H1, H2, F1, and F2 alloys these graphics are given in Figure 5.15. These plots show how the activation energies change between alloys by heating rate. By taking linear fit on these plots the slope values were obtained and by putting these values in the right side of the equation the activation energies were found as 402 kJ/mol, 59.61 kJ/mol, 264.26 kJ/mol and 362.51 kJ/mol for H1, H2,F2, and F1 alloy, respectively. Here, H1 alloy has the highest activation energy value, and H2 alloy has the lowest, decrease of the activation energy affected by decreasing of Mn fraction element.

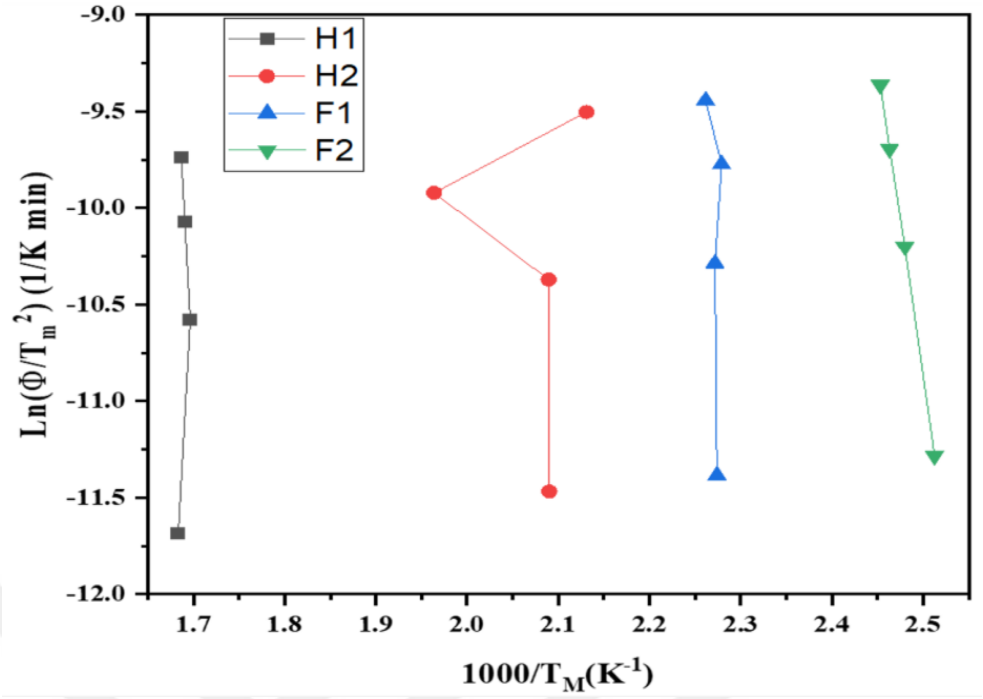

Figure 5.15. Activation energy change plots of all alloy samples.

5.5. Thermogravimetric/ Differential Thermal Analysis (TG/DTA)

By cooling from high-temperature β phase region, Cu-Al based SMAs undertake a sequence of ordering reactions as β(A2) $\rightarrow\beta_2$(B2) $\rightarrow\beta_1$(L2$_1$) [51] which can be observed on the DTA (differential thermal analysis) thermograms of these alloys, and reversely by heating. Here, DTA measurements were taken at the heating/cooling rate of 25 °C/min for F1, F2 and H1 alloys, and at the heating/cooling rate of 45 °C/min for H2 alloy and the results are shown as thermograms for F1, F2, H1 and H2 alloys in Figures 5.16-5.19, respectively. According to the DTA patterns of F1 and F2 alloy respectively shown in Figure 5.16 and Figure 5.17, the endothermic peaks seen on the far-left side of the heating parts of these DTA cycles indicates *18R→L2$_1$(DO$_3$)* phase transitions and the peaks of eutectoid reactions can be seen at around 550 ^{o}C and then some up-down flexions seen at around 800^{o}C refer to B2→A2 transitions [52, 53].

The results of the DTA measurements given in Figure 5.18. taken at heating rate of 25 °C/min (without cooling part) for H1 alloy and in Figure 5.19. taken at 45°C/min of heating/cooling rate for H2 alloy show that the first downward endothermic peaks on the left side of these patterns at around 320°C and 200°C for H1 and H2 alloy, respectively, indicate direct *$\beta1'$*(18R)→*$\beta1$*(L2$_1$) transformations. At between 400 °C - 500 °C we can observe the decomposition of β1 phase at first into a metastable B2 *(β2)* then into the admixture of γ2 and *α* precipitation phases [52, 53]. At around 520 °C to 550 °C there can be seen the eutectoid reaction peaks.

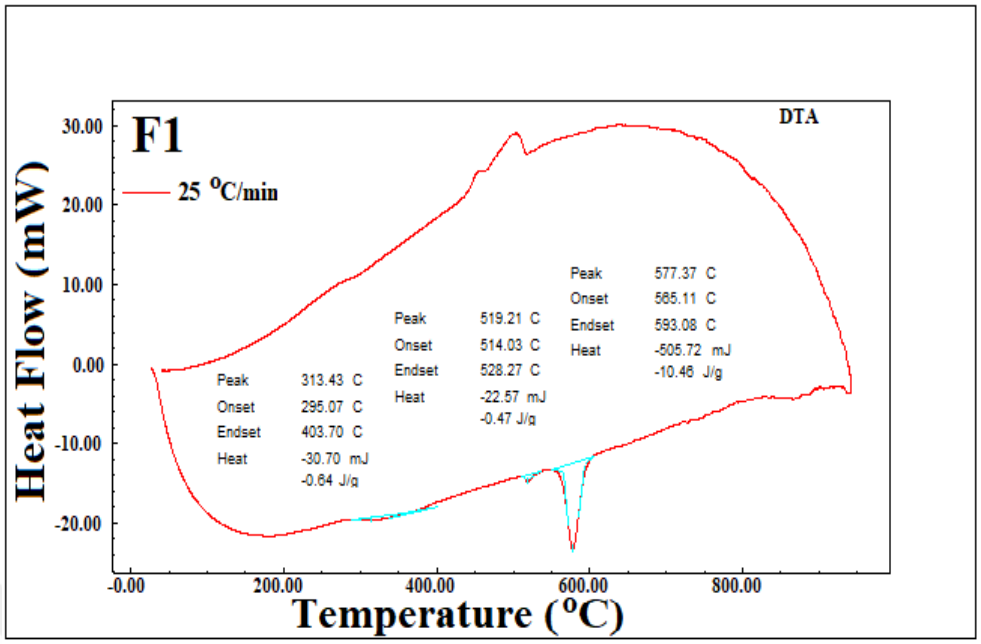

Figure 5.16. DTA result for F1 alloy.

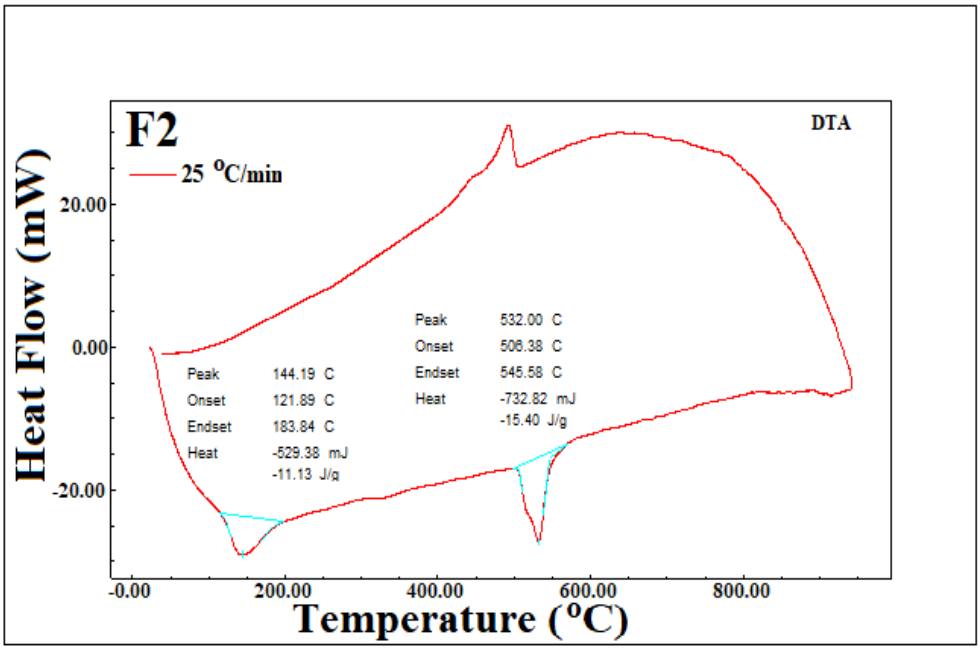

Figure 5.17. DTA result for F2 alloy.

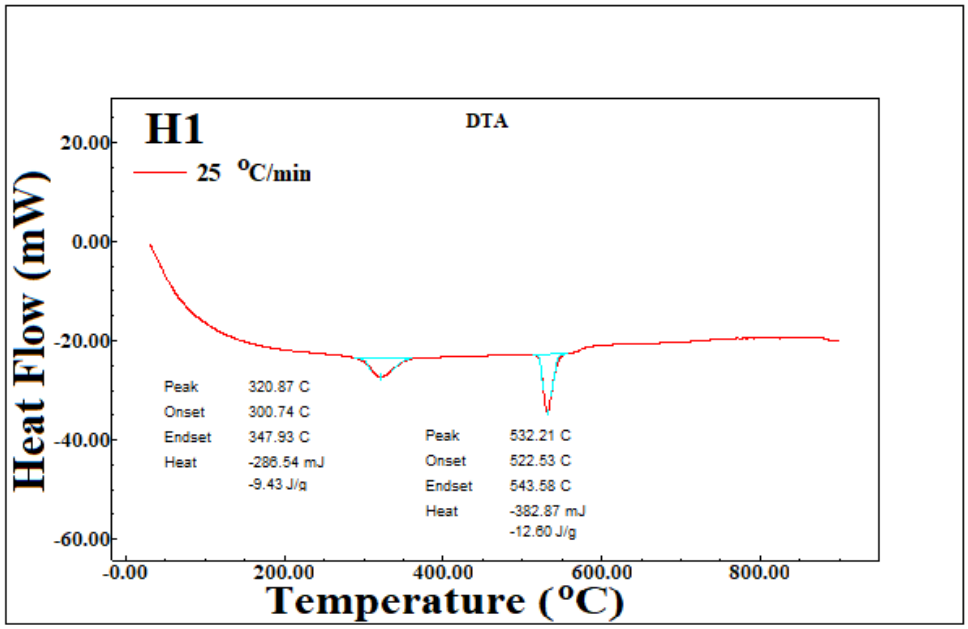

Figure 5.18. DTA heating pattern of H1 alloy.

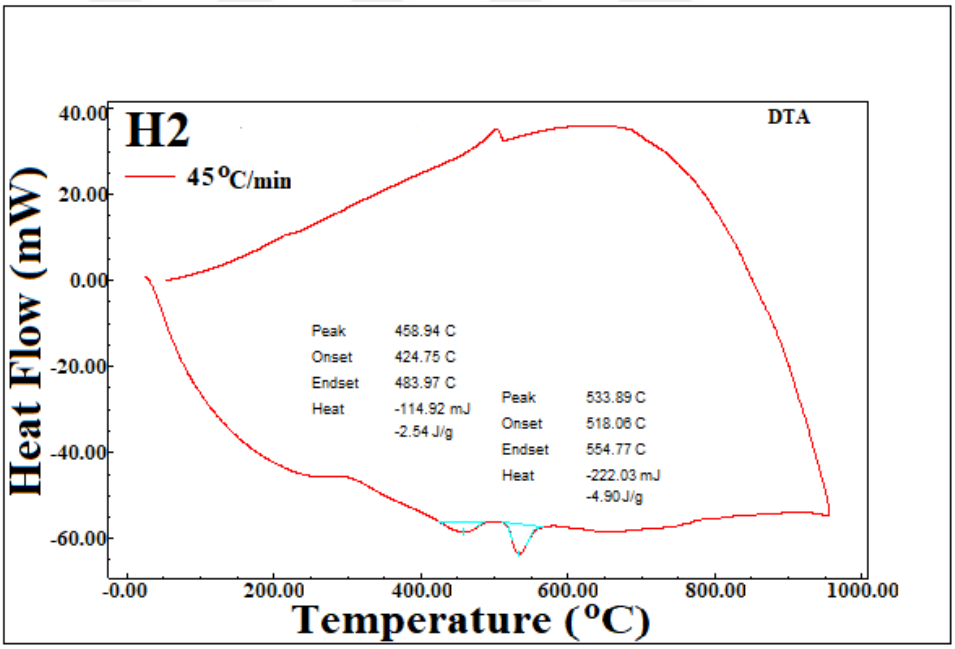

Figure 5.19. DTA heating pattern of H2 alloy.

5.6. X-Ray Diffraction (XRD)

X-ray measurements for all of the alloy samples were taken at room temperature according to using Rigaku RadB-DMAX II diffractometer. The results are given in Figure 5.20. The maximum intensity peaks indicating the monoclinic 18R martensite phase observed at 2Θ=44.48° and 40.06° came up for H2 is (1210), for H1 is (122). Furthermore, the other peaks of (122), (2012) and β1'(042) planes [47] were seen in both samples and a γ1′(222) peak representating 2H

martensite was also noticed only for H1 alloy. And the peaks of (1210) plane indicating β1' martensite phase were detected at 2Θ=44.72° and 44.77° for F2 and F1 alloys, respectively. The other peaks for F1 are *β1'*(122) and *β1'*(042), while they are β1'(042), *β1'*(2012), *β1'*(122) and *β1'*(0022) for F2 sample [52, 53]. As it is noticed that the *β1'*(0022) and *β1'*(2012) peaks on the pattern of F2 alloy became vanished on the pattern of F1 alloy. Furthermore, the further peaks on the pattern of F2 alloy significantly shrink on the pattern of F1 sample due to the higher Be, Mn and lower Al content in the F1 alloy, as shown in Figure 5.21.

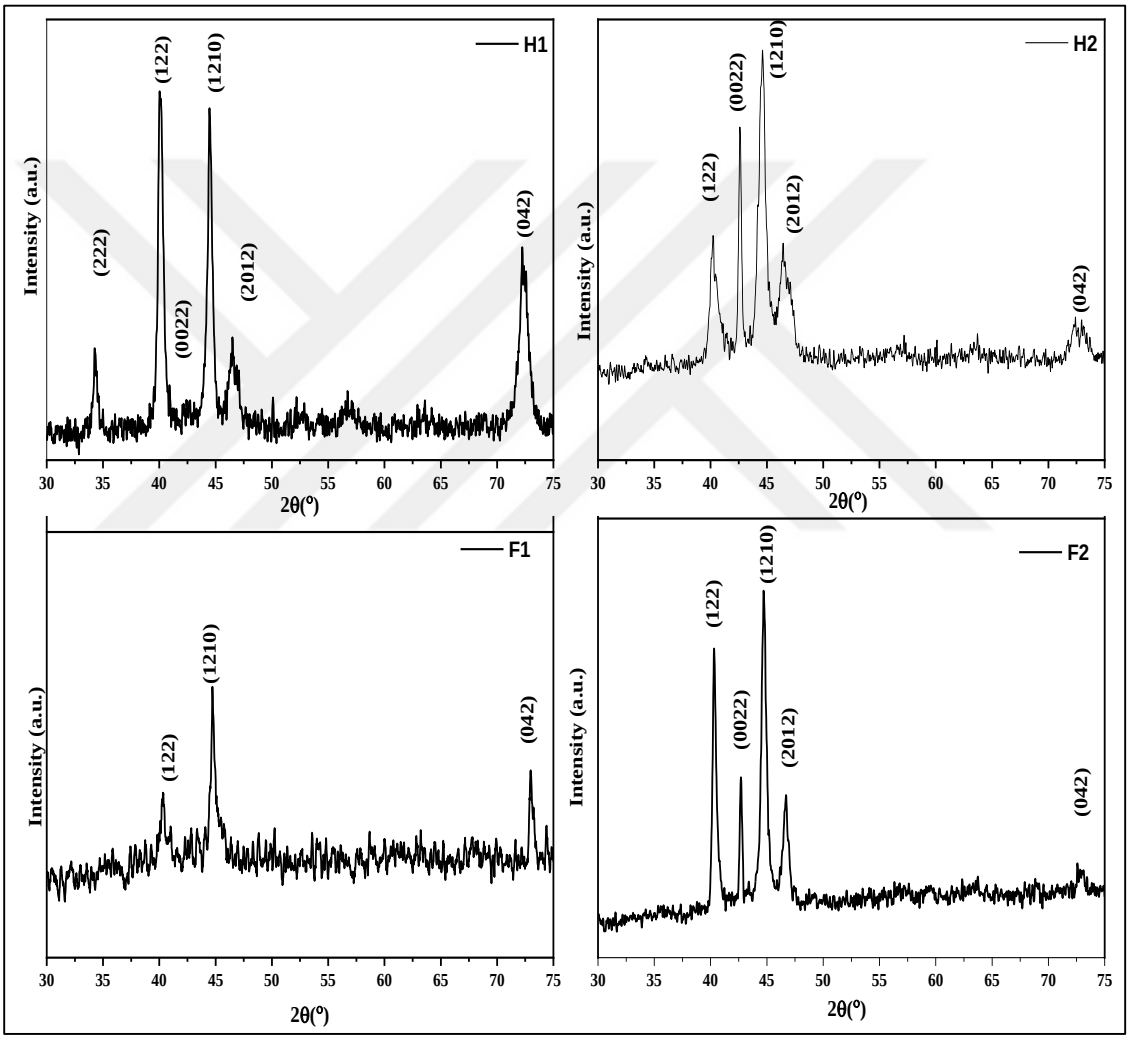

Figure 5.20. XRD results for H1, H2, F1, and F2 alloy samples.

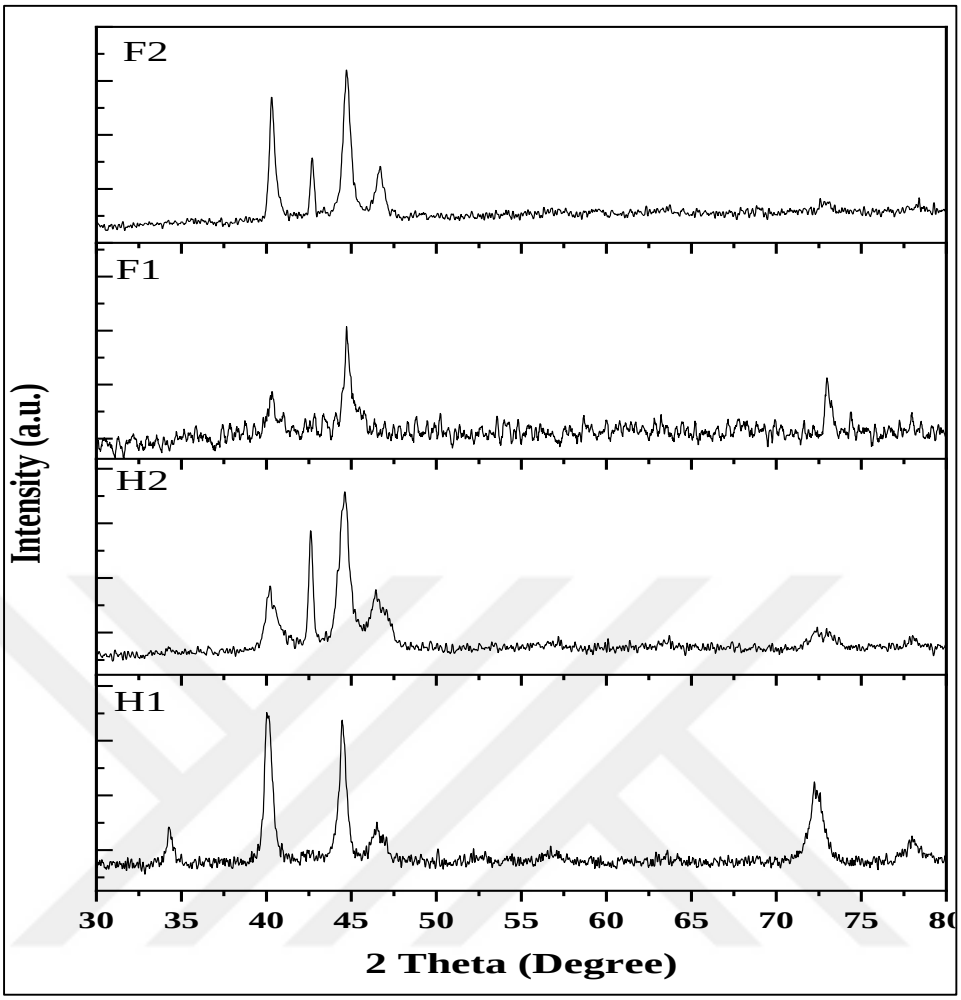

Figure 5.21. Comparison of the differences between XRD patterns of the alloy samples.

The average crystallite size (*D*) for each alloy can be calculated by using XRD diffraction information of alloy samples by using the Debye-Scherer equation [52, 53] as given below;

$$D = \frac{0.9\,\lambda}{B_{1/2}\cos\theta} \tag{5.2}$$

where; θ is the Bragg angle, λ is the wavelength of the X-ray CuKα radiation (λ=0.15406), *D* is average crystallite size and $B_{1/2}$ is the peak full width at half maximum (FWHM). Furthermore, the crystallite size values were found for each alloys as 20.76 nm, 19.139 nm, 17.66 nm, and 14.55 nm for F1, F2, H1, and H2 alloys, respectively. Lowered Al content and Mn addition in H2 alloy decreased its crystallite size.

6. CONCLUSIONS

In this work, four different shape memory alloys, one CuAlFe, one CuAlFeMn, and two CuAlBeMn alloys, with new unprecedented compositions were prepared with the arc-melting method. Structural properties and characteristic thermal parameters of these alloys were investigated by conducting a series of measurements to reveal whether shape memory effect and other SMA properties exist in them or not. As a result of thermal DSC/DTA measurements, all of the alloys exhibited direct and reverse martensitic phase transformation peaks above 100 °C and below 400 °C, therefore they were estimated as high-temperature shape memory alloys (HTSMAs), which are considered in the first group of HTSMAs. DSC results for all of the alloys showed that all of the thermodynamic parameters of the alloys were changed by the effects of compositional changes and found very sensitive to the varied contents of additive elements. The transformation temperatures were observed varying at between 122 °C and 346 °C for each alloy. The transformation temperatures and the thermodynamic parameters for instance the entropy, $(A_f - M_s)$ hysteresis values and enthalpy were noticed very sensitive to the variations content in Al, Be, and Mn, they decreased by Mn addition and increased by an increment in Al content. For CuAlBeMn alloys, at least 7.34% lower Be, with 64.8% lower Mn and 45% more Al contents led to a significant decrease in all of their hysteresis values and transformation temperatures. Such parameters decreased by Mn addition to CuAlFe alloy, while a higher Al content (without Mn) increased them in CuAlFe alloy, so that by adding a minor amount of Mn to CuAlFe and making a small compositional change in the ternary alloy base the martensite transformation temperatures of CuAlFeMn alloy became to be increased approximately 100 °C.

The X-ray measurements for all of the alloys showed the maximum intensity peaks indicating the monoclinic 18R martensite phase on their diffraction patterns that confirmed the formation of martensite in these alloys. X-ray diffraction peaks were found very sensitive to the compositional changes and additional contents, as well. Changes in the intensities of main and ordinary XRD peaks on the diffraction patterns of the CuAlFeMn alloy happened mainly due to the reducing of Al and addition of Mn content, in CuAlFe alloy and the crystallite size decreased due to Mn addition and lesser Al content. In the Be group of CuAlBeMn alloys, X-ray diffraction patterns and crystallite size values were all varied with the change of composition, too.

Optical micrographs imaging the surface morphologies of the alloys displayed the needle-shaped 18R(β1`) martensite phase exists together with the 2H(γ1`) martensite forms which proved the predictions made by the calculated average e/a electron concentration values of the alloys, the XRD results confirmed this prediction, too. The precipitations observed on the alloys' surfaces formed due to Mn, Fe, and Be contents.

REFERENCES

[1] Mehta, K. and Gupta, K., (2019). *Fabrication and processing of shape memory alloys*, Springer Cham, Switzerland.

[2] Laureanda, C., (2008). *One Way and Two Way–Shape Memory Effect: Thermo–Mechanical Characterization of Ni–Ti wires*, Ph. D. thesis, Universitá degli Studi di Pavia.

[3] Stöckel, D. (1995). The shape memory effect-phenomenon, alloys and applications. *Proceedings: Shape Memory Alloys for Power Systems EPRI*, 1, 1-13.

[4] Noyan, E. (1990). *Shape Memory Alloy Design*, Doctor Of Philosophy Thesis, Middle East Technical University, Ankara.

[5] Krishnan, V.B. (2004). Design, fabrication and testing of a shape memory alloy based cryogenic thermal conduction switch. Master thesis. Electronic Theses and Dissertations, 2004-2019. 100. University of Central Florida. https://stars.library.ucf.edu/etd/100

[6] Ahmed, H.M., Canbay, C.A., and Özkul, İ., (2019). *Fabrication of quaternary high temperature shape memory alloys*. in *AIP Conference Proceedings*. AIP Publishing.

[7] Ma, J., Karaman, I., and Noebe, R.D. (2010). High temperature shape memory alloys, *International Materials Reviews*, C 55, 257-315.

[8] Lobo, P.S., Almeida, J., and Guerreiro, L. (2015). Shape memory alloys behaviour: A review, *Procedia Engineering*, C 114, 776-783.

[9] Laureanda, C., (2008). *One Way and Two Way–Shape Memory Effect: Thermo–Mechanical Characterization of Ni–Ti wires*. Master thesis, Universita´ Degli Studi di Pavia.

[10] Andreasen, G.F. (1977). *Method and system for orthodontic moving of teeth*. US Patents; US4037324A.

[11] Mihálcz, I. (2001). Fundamental characteristics and design method for nickel-titanium shape memory alloy, *Periodica Polytechnica Mechanical Engineering*, C 45, 75-86.

[12] Czechowicz, A. and Langbein, S., (2015). *Shape memory alloy valves: Basics, potentials, design*, Springer International Publishing Switzerland.

[13] Mellor, B., Guilemany, J., and Fernandez, J. (1991). Two way shape memory effect obtained by stabilised stress induced martensite in Cu-Zn-Al-Co and Cu-Al-Mn alloys, *Le Journal de Physique IV*, C 1, C4-457-C4-462.

[14] Mehrpouya, M. (2013). *Modeling of Machining Process of Nickel-Titatium Based Shape Memory Alloy*. Master thesis, Universiti Putra Malaysia

[15] Al-Humairi, S.N. Saud, (2019). *Cu-based shape memory alloys: modified structures and their related properties*, Book Chapter in: Recent Advances in Engineering Materials and Metallurgy, IntechOpen, 10.5772/intechopen.86193.

[16] Bhadeshia, H., (2001). *Martensitic transformation*, Trans Tech Publ. p. 5203-5206.

[17] Otsuka, K. and Kakeshita, T. (2002). Science and technology of shape-memory alloys: new developments, *mrs bulletin*, C 27, 91-100.

[18] Otsuka, K. and Wayman, C. (1998). Mechanism of shape memory effect and superelasticity, *Shape memory materials*, C, 27-48.

[19] Bujoreanu, L., Stanciu, S., Özkal, B., Comăneci, R., and Meyer, M. (2009). *Comparative study of the structures of Fe-Mn-Si-Cr-Ni shape memory alloys obtained by classical and by powder metallurgy, respectively*. in *European Symposium on Martensitic Transformations*. EDP Sciences.

[20] Liu, Y. (2001). *Detwinning process and its anisotropy in shape memory alloys*, Proc. SPIE Smart Mater., vol. 4234, pp. 82-93. https://doi.org/10.1117/12.424392

[21] Pascover, J. and Radcliffe, S. (1971). The thermodynamics of martensitic transformation, *Metallurgical Transactions*, C 2, 2387.

[22] Aksu Canbay, C. (2010). Bakır Bazlı Şekil Hatırlamalı Alaşım Üretimi ve Alaşımların Yapısal, Termal ve Elektriksel Özelliklerinin İncelenmesi, Fırat Üniversitesi, *Fen Bilimleri Enstitüsü*, C.

[23] Canbay, C.A. and Aydoğdu, A. (2013). Thermal analysis of Cu-14.82 wt% Al-0.4 wt% Be shape memory alloy, *Journal of thermal analysis and calorimetry*, C 113, 731-737.

[24] James, R.D. and Hane, K.F. (2000). Martensitic transformations and shape-memory materials, *Acta materialia*, C 48, 197-222.

[25] Jani, J.M., Leary, M., Subic, A., and Gibson, M.A. (2014). A review of shape memory alloy research, applications and opportunities, *Materials & Design (1980-2015)*, C 56, 1078-1113.

[26] Gustmann, T., Dos Santos, J., Gargarella, P., Kühn, U., Van Humbeeck, J., and Pauly, S. (2017). Properties of Cu-based shape-memory alloys prepared by selective laser melting, *Shape Memory and Superelasticity*, C 3, 24-36.

[27] Acitei, D. C., Sandhu, A. V., Abdullah, M. M. A. B., Vizureanu, P., & Abdullah, A. (2013). On the Structure of Shape Memory Alloys. Key Engineering Materials, 594–595, 140–145. https://doi.org/10.4028/www.scientific.net/kem.594-595.140

[28] Cladera, A., Weber, B., Leinenbach, C., Czaderski, C., Shahverdi, M., and Motavalli, M. (2014). Iron-based shape memory alloys for civil engineering structures: An overview, *Construction and building materials*, C 63, 281-293.

[29] Jani, J. M., Leary, M., & Subic, A. (2014). *Shape Memory Alloys in Automotive Applications*. Applied Mechanics and Materials, 663, 248–253. https://doi.org/10.4028/www.scientific.net/amm.663.248

[30] R. A. Russell and R. B. Gorbet, (1995). *Improving the response of SMA actuators*, Proc. IEEE International Conference on Robotics and Automation, Nagoya, Japan, pp. 2299-2304 vol.3, doi: 10.1109/ROBOT.1995.525604

[31] Langbein, S. (2009). *Development of standardised and integrated shape memory components in "one-module"-design*. in *European Symposium on Martensitic Transformations*. ESOMAT 2009, 07010. https://doi.org/10.1051/esomat/200907010

[32] Mabe, J., Calkins, F., and Butler, G. (2006). *Boeing's variable geometry chevron, morphing aerostructure for jet noise reduction*. in *47th AIAA/ASME/ASCE/AHS/ASC Structures, Structural Dynamics, and Materials Conference 14th AIAA/ASME/AHS Adaptive Structures Conference 7th*.

[33] Sreekumar, M., Nagarajan, T., Singaperumal, M., Zoppi, M., and Molfino, R. (2007). Critical review of current trends in shape memory alloy actuators for intelligent robots, *Industrial Robot: An International Journal*, C 34, 285-294.

[34] Song, C. (2010). History and current situation of shape memory alloys devices for minimally invasive surgery, *The Open Medical Devices Journal*, 2: 24-31. DOI: 10.2174/1875181401002020024

[35] Mantovani, D. (2000). Shape memory alloys: Properties and biomedical applications, *JOM*, C 52, 36-44.

[36] Hodgson, D.E., Ming, W., and Biermann, R.J. (1990). Shape memory alloys, *ASM International, Metals Handbook, Tenth Edition.*, C 2, 897-902.

[37] Buehler, W.J. and Wang, F.E. (1968). A summary of recent research on the nitinol alloys and their potential application in ocean engineering, *Ocean Engineering*, C 1, 105-120.

[38] Morgan, N. (2004). Medical shape memory alloy applications—the market and its products, *Materials Science and Engineering: A*, C 378, 16-23.

[39] https://chem.libretexts.org/Courses/Franklin_and_Marshall_College/Introduction_to_ Materials_Characterization__CHM_412_Collaborative_Text/Spectroscopy/Energy-Dispersive_X-ray_Spectroscopy_(EDS), Access date: 03 August 2020.

[40] Andrei A. Bunaciu, Elena gabriela Udriştioiu & Hassan Y. Aboul-Enein (2015) X-Ray Diffraction: Instrumentation and Applications, Critical Reviews in Analytical Chemistry, 45:4, 289-299, DOI: 10.1080/10408347.2014.949616

[41] Jauncey, G. (1924). The scattering of x-rays and Bragg's law, *Proceedings of the National Academy of Sciences of the United States of America*, C 10, 57.

[42] Speakman, S.A. (2011). Basics of X-ray powder diffraction, *Massachusetts-USA, 2011a. Disponível em:<http://prism. mit. edu/xray/Basics% 20of% 20X-Ray% 20Powder% 20Diffraction. pdf>*, Access date: 3 August 2020.

[43] Duong, D.L., Han, G.H., Lee, S.M., Gunes, F., Kim, E.S., Kim, S.T., Kim, H., Ta, Q.H., So, K.P., and Yoon, S.J. (2012). Probing graphene grain boundaries with optical microscopy, *Nature*, C 490, 235.

[44] Schick, C. (2009). Differential scanning calorimetry (DSC) of semicrystalline polymers, *Analytical and bioanalytical chemistry*, C 395, 1589.

[45] Canbay, C.A., (2010). *The production of Cu-based shape memory alloys and investigation of microstructural, thermal and electrical properties of alloys*, Ph. D Thesis, Fırat University, Institute of Science, Elazıg/Turkey (Turkish).

[46] Francioso, O., Montecchio, D., Gioacchini, P., and Ciavatta, C. (2005). Thermal analysis (TG–DTA) and isotopic characterization (13C–15N) of humic acids from different origins, *Applied Geochemistry*, C 20, 537-544.

[47] Lagoudas, D.C., (2008). *Shape memory alloys: modeling and engineering applications*, Springer, Boston, MA. https://doi.org/10.1007/978-0-387-47685-8

[48] Ünlü, N., Canbay, C.A., Ozkul, İ., and Karaduman, O. (2019). Smart material characterization by thermal and structural analysing techniques. *AIP Conference Proceedings* 2178, 030032 https://doi.org/10.1063/1.5135430.

[49] Prado, M O, et al.,(1995). Martensitic transformation in Cu-Mn-Al alloys. Scripta Metallurgica et Materialia, Volume 33, Issue 6, Pages 877-883. DOI: 10.1016/0956-716X(95)00292-4

[50] Ahlers, M. (1995). Phase stability of martensitic structures, *Le Journal de Physique IV*, C 5, C8-71-C8-80.

[51] Mallik, U. and Sampath, V. (2008). Effect of alloying on microstructure and shape memory characteristics of Cu–Al–Mn shape memory alloys, *Materials Science and Engineering: A*, C 481, 680-683.

[52] Canbay, C.A., Karaduman, O., Ünlü, N., Baiz, S.A., and Özkul, İ. (2019). Heat treatment and quenching media effects on the thermodynamical, thermoelastical and structural characteristics of a new Cu-based quaternary shape memory alloy, *Composites Part B: Engineering*, C, 106940. https://doi.org/10.1016/j.compositesb.2019.106940

[53] Mallik, U. and Sampath, V. (2008). Effect of composition and ageing on damping characteristics of Cu–Al–Mn shape memory alloys, *Materials Science and Engineering: A*, C 478, 48-55.

CURRICULUM VITAE

Hiwa Mustafa AHMED

PERSONAL INFORMATIONS

Birth of Place : Sulaymaniyah-Iraq
Birth of Date : 04-04-1984
Nationalty : Iraqi
Address : Sulaymaniyah - Iraq
E-mail : hiwa.mustafa@raparinuni.org
Languages : English B2, Kurdish C1, Arabic A2 and Turkish A2

EDUCATION

Bachelor : University of Koya, Faculty science & Health, Department of Physics, 2011
High School : 5thAZAR, Ranyah-Sulaymaniyah-Iraq, 2007

RESEARCH EXPERIENCES

- ✓ Laboratory Instruments you use, such as X-ray crystallography, oscilloscope, optical spectrometer ….
- ✓ Computer Programming languages available (MATLAP, ENDNOTE, ORIGINLAB)

WORK EXPERIENCE

2011-2012 I worked as a teacher in secondary school.
2012–2018 I worked at university labs (AC LAB, DC LAB, Mechanic lab electronic lab and optic lab**)**

ACADEMIC ACTIVITIES

1. Ahmed, H.M., C.A. Canbay, and İ. Özkul. (2019). Fabrication of quaternary high temperature shape memory alloys. *AIP Conference Proceedings*. AIP Publishing LLC.
2. Canbay, C.A., İ. Ozkul, and H.M. Ahmed. (2019). The ternary and quaternary systems in Cu-based shape memory alloys. *AIP Conference Proceedings*. AIP Publishing LLC.